Dissecting the genetic regulation of lateral root development in tomato under salt stress

Maryam Rahmati Ishka[1], Hayley Sussman[1], Jiantao Zhao[1,] Eric Craft[2], Li'ang Yu[1], Andrew Nelson[1], Miguel Pineros[2], Mark Tester[3], Dorota Kawa[4], Zhangjun Fei[1], Magdalena M. Julkowska[1,3*]

email + ORCID:

Maryam Rahmati Ishka[1], - ORCID - 0000-0002-5447-643X - mri23@cornell.edu

Hayley Sussman[1], - ORCID - 0000-0002-1331-3319 - hs995@cornell.edu

Jiantao Zhao[1] , - ORCID - 0000-0002-5140-8220 - jz426@cornell.edu

Eric Craft[2], - ORCID - 0000-0003-0966-8296 - ejc35@cornell.edu

Li'ang Yu[1], - ORCID - 0000-0002-9556-011X - ly76@cornell.edu

Andrew Nelson[1], - ORCID - 0000-0001-9896-1739 - an425@cornell.edu

Miguel Pineros[2], ORCID - 0000-0002-7166-1848 - map25@cornell.edu

Mark Tester[3], - ORCID - 0000-0002-5085-8801 mark.tester@kaust.edu.sa

Dorota Kawa[4], - ORCID - 0000-0002-4227-1621 d.kawa@uu.nl

Zhangjun Fei[1,] ORCID - 0000-0001-9684-1450 - zf25@cornell.edu

Magdalena M. Julkowska[1,3] - ORCID - 0000-0002-4259-8296

* correspondence - mmj55@cornell.edu

Affiliations:

1 - Boyce Thompson Institute, Ithaca, NY, USA

2 - USDA-ARS, Ithaca, NY, USA

3 - Center for Desert Agriculture, King Abdullah University of Science and Technology, Thuwal, Saudi Arabia

4 – Environmental and Computational Plant Development & Plant Stress Resilience, Utrecht University, Utrecht, The Netherlands

Abstract

Tomatoes are crucial for global food security and agricultural economies. With over 50% of arable land projected to become saline by 2050, understanding tomato responses to saline environments is essential. Soil salinization, prevalent in arid regions, leads to salt stress. Roots are primary salinity sensors and integrate stress responses like nutrient deficiency. Understanding the molecular processes maintaining root growth is vital for crop resilience. While salt stress impacts on tomato seed germination, shoot growth, and fruit yield are documented, root development remains underexplored. Most studies have focused on a limited number of cultivars and their physiological responses, not the genetic basis of salt resilience. Wild tomato relatives, such as *Solanum pimpinellifolium*, offer traits that are beneficial for breeding resilient crops. However, few studies have examined the genetics of salinity tolerance in *S. pimpinellifolium*. This study characterizes salt stress-induced changes in root system architecture (RSA) using a natural diversity panel of 220 wild tomato accessions. We identified natural variation in lateral root development and several candidate loci through Genome-Wide Association Study (GWAS). Bulk segregant analysis (BSA) revealed 22 candidate genes overlapping with GWAS findings. Exploring root transcriptome reprogramming in two accessions with differing lateral root responses highlighted genotype-specific changes. Integrating GWAS, BSA, and RNA sequencing data identified four key genes underlying differential lateral root development under salt stress. These findings offer novel genetic targets for improving salt resilience in tomatoes, providing opportunities for future research and breeding programs to enhance crop sustainability and productivity.

Introduction

Tomatoes are one of the most widely cultivated and economically significant crops globally, contributing substantially to food security and agricultural economies. With projections indicating that over 50% of arable land will become saline by 2050, understanding tomato responses to diverse saline environments becomes paramount [1]. Salt stress prevails in arid regions characterized by evaporation rates exceeding freshwater input, leading to increased salt accumulation in the soil [2–4]. These dryland areas, including regions in South America, southern and western Australia, Mexico, southwest United States, and South Africa, have been identified as significant hotspots for soil salinization [5]. Additionally, salt interactions with clay particles result in impenetrable claypan that prevents roots from reaching deeper soil levels [6].

Roots are the primary site of salinity sensing and serve to integrate salt stress with other stressors like nutrient deficiency. The susceptibility of roots to salt stress determines the plant's overall productivity [7,8]. Therefore, understanding the molecular processes leading to maintained root growth is necessary for enhancing crop environmental resilience. Although the effects of salt stress on tomato plants have been studied in the context of seed germination, shoot growth, and fruit yield [9–12], the impact of salt stress on root development remains unexplored. Furthermore, previous studies have primarily concentrated on a limited number of cultivars and assessed physiological responses [11], rather than elucidating the genetic basis of salt resilience. With freshwater scarcity rising, comprehending salt stress resilience mechanisms, especially root-derived tolerance mechanisms, is crucial for enhancing global agricultural productivity and sustainability [13,14].

Wild relatives of crops possess valuable traits such as disease resistance, stress tolerance, and nutritional quality, which can be introduced into cultivated varieties through breeding programs [15–19]. Understanding the genetic basis of these traits in wild relatives facilitates the development of more resilient and sustainable crop varieties, which are crucial for ensuring food security in the face of environmental challenges. The closest wild relative of cultivated tomato, *Solanum pimpinellifollium* [20], shows high tolerance to many biotic and abiotic stresses [21], [22–27]. However, only a few studies

explored the genetics underlying salinity tolerance within *S. pimpinellifolium* natural diversity panels [12,28,29].

Here, we characterized salt stress-induced changes in the root system architecture (RSA) of a wild tomato natural diversity panel consisting of 220 *S. pimpinellifolium* accessions. We have identified natural variation mainly pertaining to lateral root development, and identified 55 putative candidate loci using Genome-Wide Association Study (GWAS). From the evaluation of the natural diversity panel, we identified two accessions with opposite root architecture responses to salt stress. We further explored the genetic components of lateral root development under salt stress using bulk segregant analysis (BSA), revealing 22 candidate genes overlapping between BSA and GWAS. Additionally, we explored reprogramming of the root transcriptome in two accessions with opposing lateral root development strategies, and identified genes that showed genotype-specific changes in response to salt stress. By intersecting GWAS, BSA and RNA-seq datasets we identified four key genes underlying differential lateral root development under salinity. Together, our investigations yielded novel genetic targets, offering opportunities for exploration and genetic discovery in tomato research and breeding.

Results

Wild tomato shows high variation in lateral root development in response to salt stress.

Using an agar plate system, we evaluated 220 *S. pimpinellifolium* accessions for their responses to salt stress (**Table S1**). The 4-day-old seedlings were transferred to media containing 0 or 100 mM NaCl and scanned daily. Although the images were collected for one week after transfer, the root architecture was quantified exclusively for the first 4 days after transfer due to root architecture complexity in a plate setup. We have calculated the daily Main Root growth rate (**Fig. 1A, Figure S1**), increase in Lateral Root number (**Fig. 1B**), and increase in average Lateral Root Length (**Fig. 1C**) using linear functions. Although salt treatment only slightly decreased the Main Root Growth Rate from 1.334 to 1.275 cm / day (**Fig. 1A**), there was a significant effect of both treatment (ANOVA p-value of 0.000157) and genotype (ANOVA p-value < 2-e16), and interaction between genotype (G) x treatment(T) (**Fig. 1D**, ANOVA *GxT* p-value of 9.56e-16). On the other hand, the Lateral Root emergence was substantially decreased by salt stress (from 4.482 to 2.219 LR / day). This interaction was also significantly affected by genotype (**Fig. 1 E**, ANOVA *GxT* p-value of 3.59e-14). Similar to the Main Root growth rate, the Lateral Root growth rate showed little decrease in response to salt stress (from 0.315 to 0.304 cm / day), and this phenotype was exclusively affected by genotype (ANOVA p-value < 2e-16), but not by environment (ANOVA p-value of 0.188) or interaction between genotype and environment (**Fig. 1F**, ANOVA *GxT* p-value of 0.383). To evaluate the extent to which root architecture is reprogrammed in response to salt stress, meaning whether individual root architecture components are affected differently, we calculated stress tolerance indices (STI) for individual growth rates (GR at 100 mM / GR at 0 mM NaCl, **Fig. 1G**). We have observed significant differences between individual root architecture components, with the increase in lateral root number being affected the most (0.494 of the control values) and average lateral root growth being affected the least (1.034 of the control value). Additionally, we have observed a significant interaction between the root architecture component and the genotype (Kruskal-Wallis p-value < 2.2e-16), indicating that the root architecture is substantially reprogrammed in response to salt stress. Within the root architecture patterns in the entire diversity panel, we have observed that the genotypes that tend to maintain a high number of lateral root numbers, tend to be compromised in their lateral root elongation, while the genotypes that tend to maintain a high lateral root elongation are oftentimes compromised in their lateral root emergence (**Fig. 1G**). These results suggest that the natural variation in *S. pimpinellifolium*'s root architecture in response to salt stress is primarily caused by its differential sensitivity to salt stress in lateral root development.

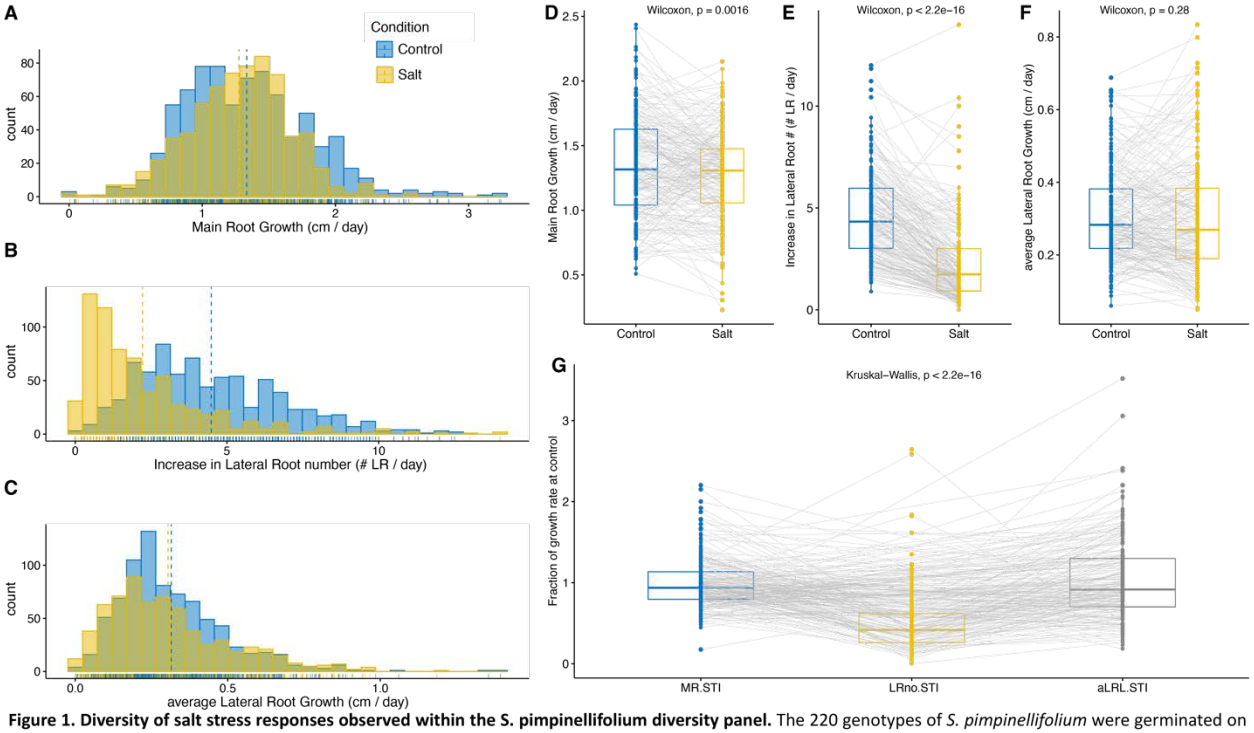

Figure 1. Diversity of salt stress responses observed within the S. pimpinellifolium diversity panel. The 220 genotypes of *S. pimpinellifolium* were germinated on ½ MS agar plates for 4 days and subsequently transferred to media containing 0 or 100 mM NaCl (Control and Salt respectively). The seedlings were imaged every 24 h after transfer for 7 consecutive days. The Root Architecture of seedlings was quantified for the first 4 days after transfer, and the **(A)** growth of Main Root, **(B)** increase in Lateral Root number and **(C)** growth of average Lateral Root was estimated using linear growth functions. The population average values for Control and Salt conditions are indicated using the dashed lines. The effect of the treatment was evaluated using a paired Wilcoxon test for **(D)** Main Root Growth Rate, **(E)** increase in Lateral Root number and **(F)** average Lateral Root Growth Rate. The individual gray lines illustrate the genotype-specific change in individual growth parameters across the conditions. **(G)** The genotype-specific growth rates at individual conditions were used to calculate the Stress Tolerance Index (STI) for individual traits, calculated by dividing growth rate estimated under Control / Salt conditions. The relative change in STI represents the salt-induced reprogramming of the root architecture. The individual gray lines represent the genotype-specific change in STI across individual components of root architecture. The individual dots represent the genotype-specific mean calculated from 4 biological replicates.

Identification of associations with tomato root architecture through GWAS.

To identify genetic components underlying the root system architecture responses to salt stress, the collected phenotypic data were combined with previously developed genotypic data [12] and used in Genome Wide Association Study (GWAS). Initially, we removed heterozygous markers, imputed the missing markers, and performed GWAS using ASReml script, similarly to the method described in [30]. This method yielded a total of 109 associated SNPs above Bonferroni threshold (LOD > 7.15), with 85 unique SNPs, grouping into 16 individual loci out of which 5 loci were associated exclusively with root architecture measured under salt stress (**Table S2**). However, this method required us to use a heavily reduced set of SNPs (708 545). Therefore, we explored additional associations using an entire set of 17 962 579 SNP using the EMMAX model with corrections for population structure (using three PCA) and kinship matrix [31]. Although no overlap was found between ASReml and EMMA-X based scripts, we identified additional 82 associations above the Bonferroni threshold (> 8.56) with various root system architecture components (**Table S2**). Only one of the significantly associated SNPs had minor allele frequency (MAF) > 1% (chromosome 1, position 1369582), associated with lateral root distribution over the length of main root (calculated as Center of Gravity) for roots grown under control conditions (**Table S2**). We further inspected associations with LOD score above 5, considering MAF, and the number of SNPs within the 10 kbp interval to select associations that can be pursued further. We have identified 55 genetic loci, each containing at least 3 SNPs within 10 kbp interval or mapped/associated with multiple root architecture traits (**Table S2**). Additionally, we have adjusted the Bonferroni threshold to 6.77 as the number of SNPs with MAF > 5% was reduced to 5 944 147.

The highest-ranking loci were identified using the biomass distribution between main and lateral roots in the first two days (MRLpTRS), including one locus on chromosome 3 consisting of 29 SNPs, three

loci on chromosome 4 consisting of 240, 39 and 85 SNPs (**Fig. 2 A - B**). Most of the SNPs on chromosome 3 were located within the coding region of *Spimp03g102810*, encoding ABC transporter A family member 7, or its promoter region (**Fig. 2C**). All the loci on chromosome 4 were neighboring each other, spanning the region between *Spimp04g130520* and *Spimp04g130690* (**Fig. 2D-F**). The highly associated SNPs were distributed throughout the entire region. The locus contained two DUF4283 proteins (*Spim04g130540* and *Spim04g130640*), one Zinc knuckle CCHC-type family protein (*Spimp04g130650*), two L-ascorbate oxidases (*Spimp04g130630* and *Spimp04g130690*), nine MADS-box containing proteins (*Spim04g130520*, *Spim04g130580*, *Spim04g130590*, *Spim04g130600*, *Spim04g130610*, *Spim04g130620*, *Spim04g130670*, *Spim04g130680*) and one MADS-box transcription factor (*Spim04g130530*), two RING domain-containing proteins (*Spimp04g130550*, *Spimp04g130660*) and one unknown protein (*Spimp04g130570*).

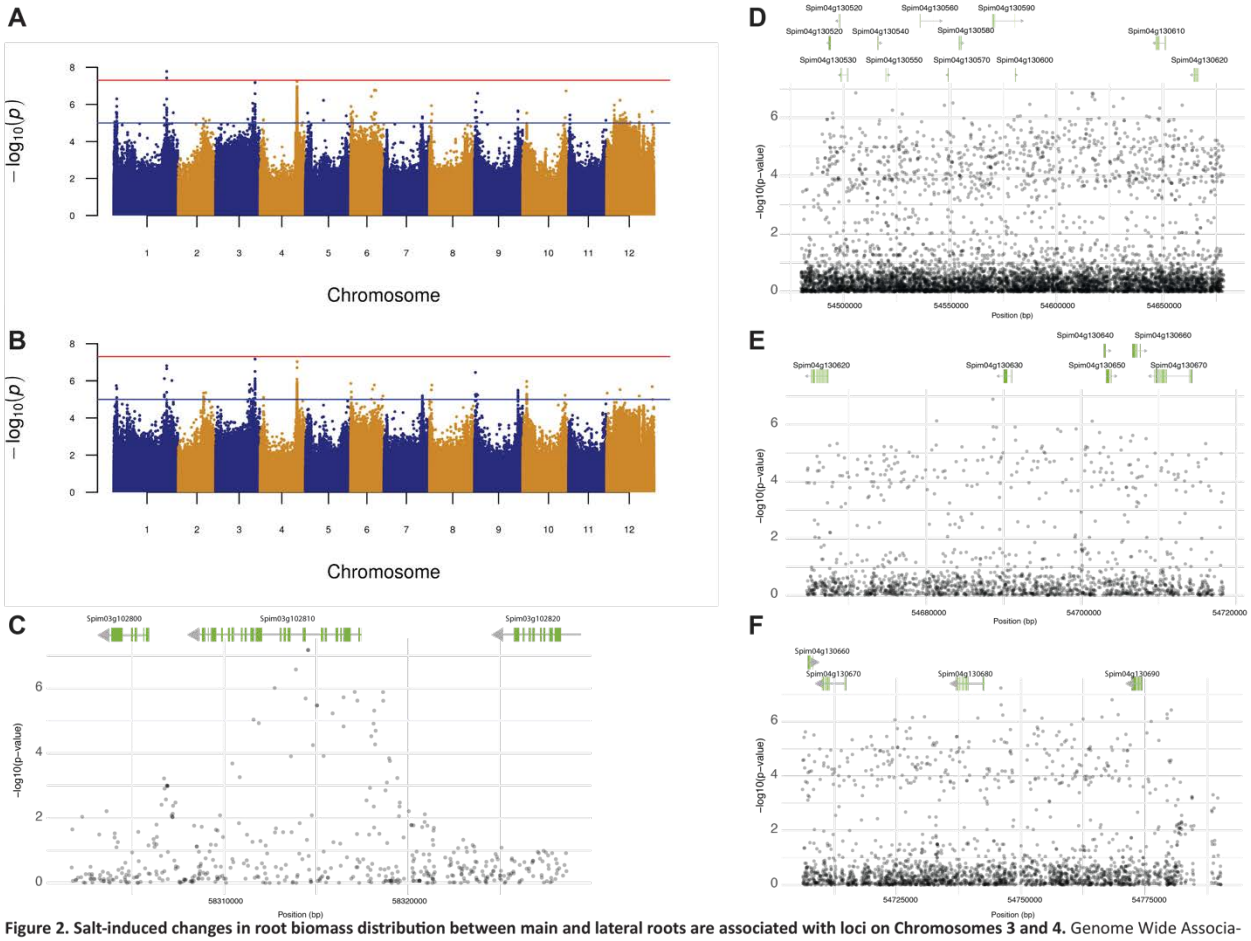

Figure 2. Salt-induced changes in root biomass distribution between main and lateral roots are associated with loci on Chromosomes 3 and 4. Genome Wide Association Study was performed on 9M SNPs using standard EMMA-X method. Only SNPs with minor allele frequency > 0.05 were used for plotting the Manhattan plot for associations identified with **(A)** ratio of main root length to total root size at 1 day and **(B)** two days post transfer to salt stress, with pseudo-heritability values of 0.116 and 0.195 respectively. The red line indicates the Bonferroni threshold, whereas the blue line indicates genome-wide suggestive threshold. **(C)** The significantly associated loci were inspected in further detail for the gene coding sequences within the regions with significantly associated SNPs. The region on chromosome 3 contained 29 SNPs with -log10(p-value) > 5. The three individual loci **(D-F)** identified on chromosome 4 contained 240, 39 and 85 SNPs with -log10(p-value) > 5. The association graph below each locus represents the association strength with the ratio of main root length to total root size at 1 day after salt stress imposition.

The second highest ranking loci were identified with lateral root length and lateral root number observed after 1 day of salt stress (**Fig. 3 A-B**). The 27 highly associated SNPs on chromosome 1 were located within the promoter region of *Spimp01g004220*, encoding a LITAF domain-containing protein (**Fig. 3C**). Three highly associated SNPs on chromosome 3 spanned three genes, *Spimp03g108680*, *Spimp03g108690* and *Spimp03g108700*, encoding a core-2/I-branching beta-1,6-N-acetylglucosaminyltransferase family protein, an AP-3 complex subunit delta and a histidine--tRNA ligase, respectively (**Fig. 3D**). On chromosome 11, we identified 60 highly associated SNPs that localized into the coding region of *Spimp11g311320*, encoding a chloroplast ribosome-recycling factor, flanked by

Spimp11g311310 and *Spimp11g311330*, encoding a bark storage protein A-like and a TsaA-like domain-containing protein, respectively.

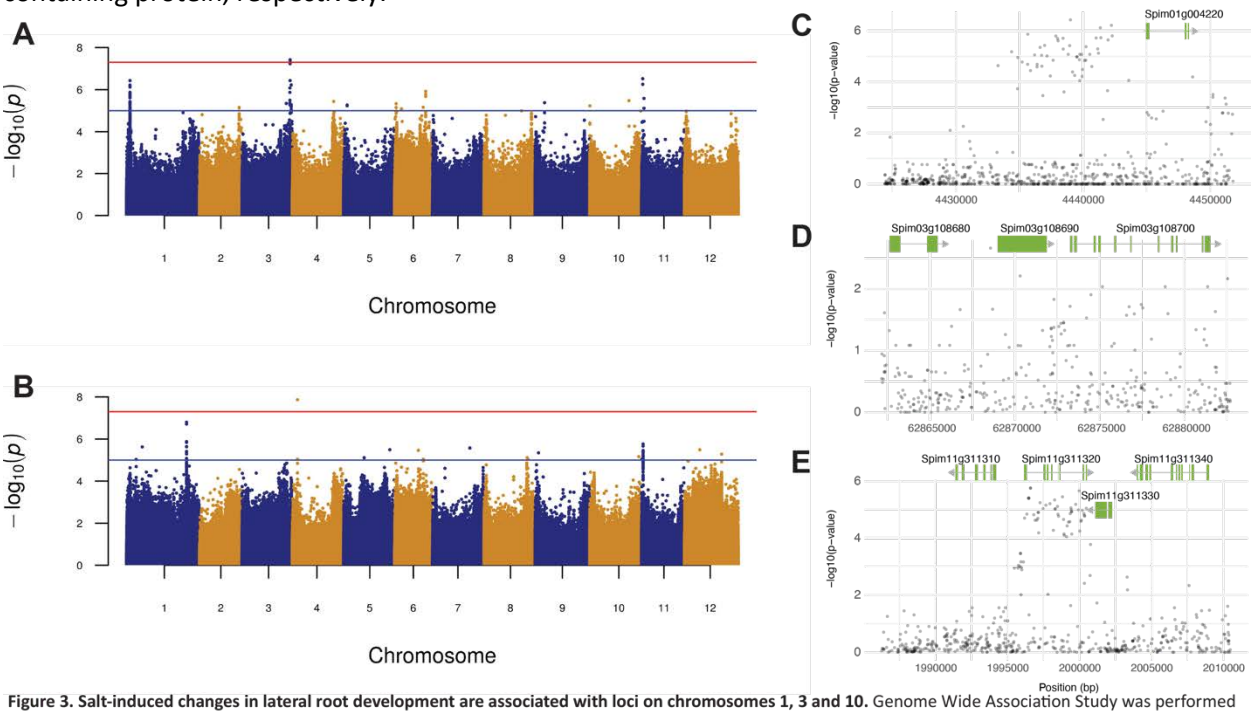

Figure 3. Salt-induced changes in lateral root development are associated with loci on chromosomes 1, 3 and 10. Genome Wide Association Study was performed on 9M SNPs using standard EMMA-X method. Only SNPs with minor allele frequency > 0.05 were used for plotting the Manhattan plot for associations identified with **(A)** average lateral root length and **(B)** lateral root number at one day post transfer to salt stress, with pseudo-heritability values of 0.145 and 0.358 respectively. The red line indicates the Bonferroni threshold, whereas the blue line indicates genome-wide suggestive threshold. **(C)** The significantly associated loci were inspected in further detail for the gene coding sequences within the regions with significantly associated SNPs. The region on chromosome 1 contained 27 SNPs, **(D)** the region on chromosome 3 7 SNPs, and (E) region on chromosome 11 contained 60 SNPs with -log10(p-value) > 5. The association graph below each locus represents the association strength with the average lateral root length at 1 day after salt stress imposition.

Two other high-ranking loci were identified with an increase in lateral root number and main root growth rate, both recorded under salt stress conditions (**Fig. 4A-B**). The 16 SNPs associated with an increase lateral root number on chromosome 12 were identified around *Spimp12g340040*, encoding a glucan endo-1,3-beta-D-glucosidase, flanked by *Spimp12g340030* and *Spimp12g340050*, encoding a ubiquitin-like domain-containing protein and a cellulose synthase CslG, respectively (**Fig. 4C**). The 15 SNPs associated with main root elongation under salt stress were located between *Spimp11g316010*, *Spimp11g316020* and *Spimp11g316030*, encoding two unknown proteins and a dephospho-CoA kinase, respectively (**Fig. 4D**).

Other loci that were identified to have more than 10 highly associated SNPs were on chromosome 5 (one locus consisting of 15 SNPs and one locus of 11 SNPs associated with number of lateral roots under Control conditions, **Fig. S2A-C**), chromosome 1 (14 SNPs associated with number of lateral roots under Control conditions, **Fig. S2D-E**), chromosome 12 (13 SNPs associated with biomass distribution between main and lateral root length under salt stress conditions, **Fig. S2F-G**) and chromosome 2 (13 SNPs associated with total root size under salt stress conditions, **Fig. S2H-I**).

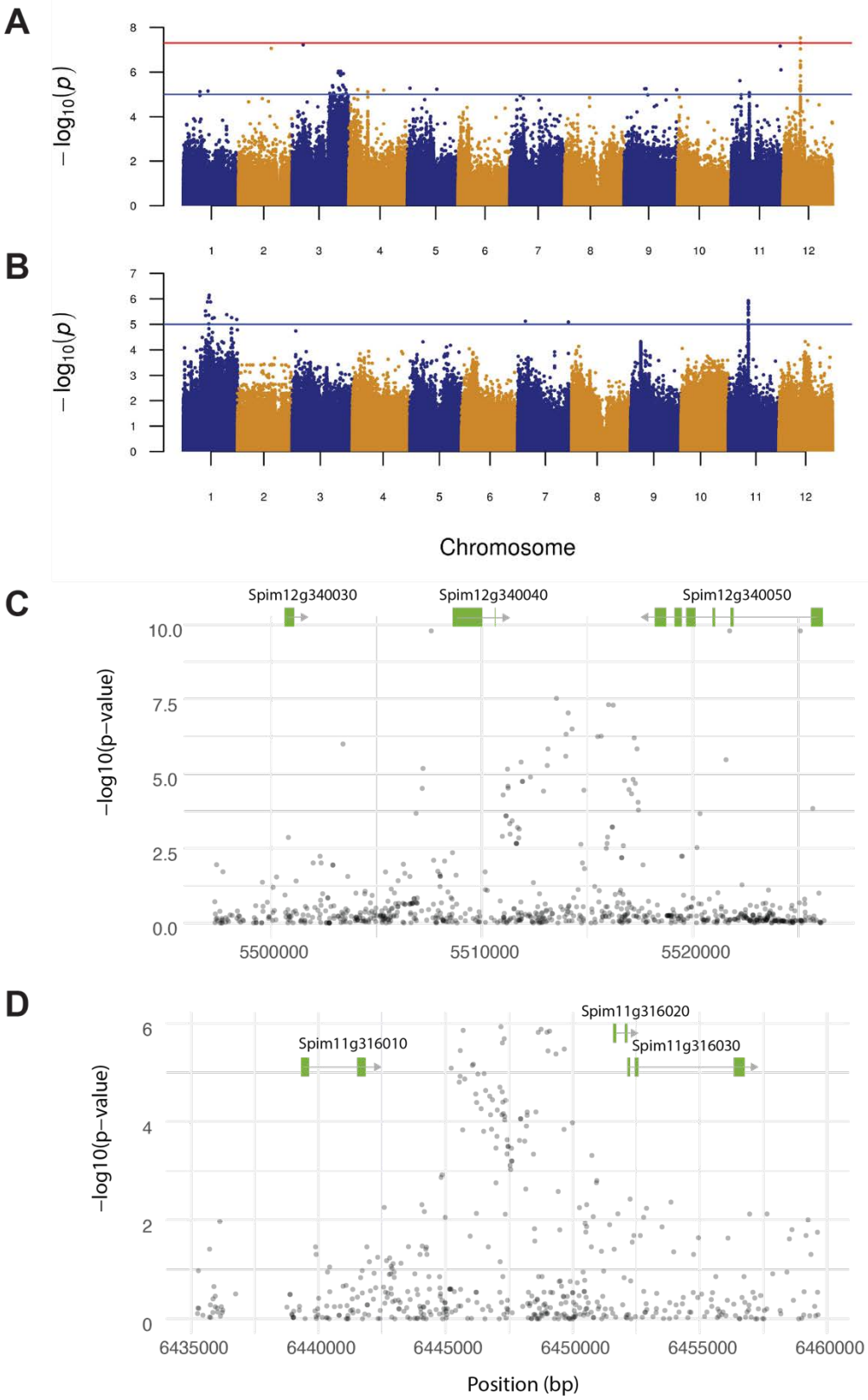

Figure 4. Emergence of lateral roots and main root growth rate is associated with loci on chromosomes 12 and 22. Genome Wide Association Study was performed on 9M SNPs using standard EMMA-X method. Only SNPs with minor allele frequency > 0.05 were used for plotting the Manhattan plot for associations identified with **(A)** lateral root emergence and **(B)** main root growth rate under salt stress, with pseudo-heritability values of 0.855 and 0.628 respectively. The red line indicates the Bonferroni threshold, whereas the blue line indicates genome-wide suggestive threshold. **(C)** The significantly associated loci were inspected in further detail for the gene coding sequences within the regions with significantly associated SNPs. The region on chromosome 12 contained 16 SNPs, whereas **(D)** the region on chromosome 11 contained 15 SNPs -log10(p-value) > 5. The association graph below each locus represents the association strength with the trait initially associated with that locus.

LA2540 and LA1511 prioritize different aspects of lateral root development under salt stress.

From the natural diversity panel, we selected two accessions to be investigated in more detail for their root system architecture responses to salt stress. We selected LA2540 as wild tolerant (referred hereafter as WT) accession, and LA1371 as wild sensitive (referred hereafter as WS) accession. Additionally, we included an *S. lycopersicum* accession (LA1511, referred hereafter as CT) to represent the cultivated tomato. LA1511 possessed similar growth characteristics as *S. pimpinellifolium* including small fruits morphology. Salt stress reduced main root growth (**Fig. 5A**), lateral root length (**Fig. 5B**), and the number of lateral roots (**Fig. 5C**) across all examined accessions. While the relative growth of the main root (calculated as Stress Tolerance Index (STI), as described above) did not differ across examined genotypes (**Fig. 5D**), substantial differences were observed between wild-tolerant and cultivated tomatoes in lateral root-related traits (**Fig. 5E-F**). Wild-tolerant accession showed a higher STI for average lateral root elongation (**Fig. 5E**), whereas cultivated accession exhibited a higher STI for lateral root emergence (**Fig. 5F**). Additionally, we have evaluated the selected genotypes for ion accumulation using ICP-AES after 10 days of exposure to salt stress (**Fig. 5G and Fig. S3**). Salt stress exposure resulted in increased and decreased Na^+ and K^+ accumulation respectively, with no significant differences between the genotypes. Although all accessions maintained a similar Na^+/K^+ ratio in the roots, cultivated tomato exhibited a significantly lower Na^+/K^+ ratio in the shoot compared to both wild accessions. Summarizing, we have identified LA1511 as a salt-tolerant *S. lycopersicum* line that prioritizes the development of new lateral roots, while LA2540 as a tolerant *S. pimpinellifolium* line prioritizes the elongation of existing lateral roots.

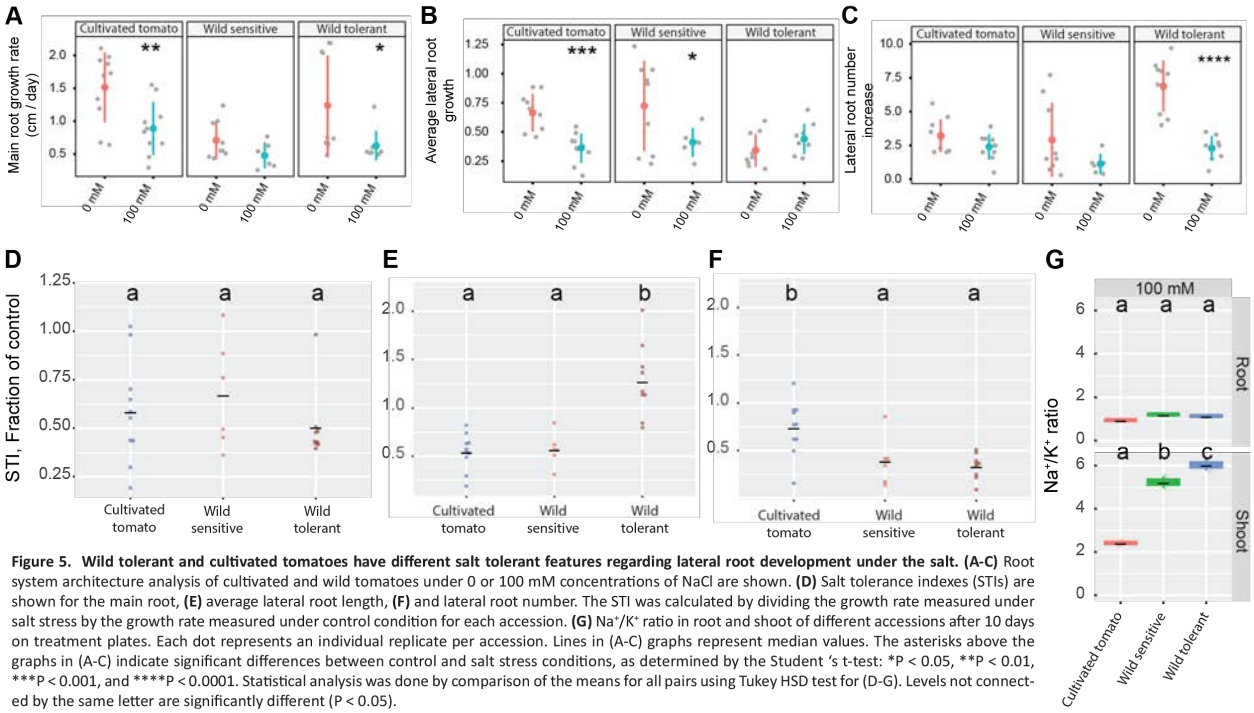

Figure 5. Wild tolerant and cultivated tomatoes have different salt tolerant features regarding lateral root development under the salt. (A-C) Root system architecture analysis of cultivated and wild tomatoes under 0 or 100 mM concentrations of NaCl are shown. **(D)** Salt tolerance indexes (STIs) are shown for the main root, **(E)** average lateral root length, **(F)** and lateral root number. The STI was calculated by dividing the growth rate measured under salt stress by the growth rate measured under control condition for each accession. **(G)** Na^+/K^+ ratio in root and shoot of different accessions after 10 days on treatment plates. Each dot represents an individual replicate per accession. Lines in (A-C) graphs represent median values. The asterisks above the graphs in (A-C) indicate significant differences between control and salt stress conditions, as determined by the Student 's t-test: *P < 0.05, **P < 0.01, ***P < 0.001, and ****P < 0.0001. Statistical analysis was done by comparison of the means for all pairs using Tukey HSD test for (D-G). Levels not connected by the same letter are significantly different (P < 0.05).

Compound effect of F1 hybrid on maintenance of lateral root development under salt stress.

To further evaluate the genetic mechanisms underlying the differential responses of lateral roots between WT and CT, and explore whether the salt tolerance mechanisms are complementary between these two accessions, we generated an F1 hybrid by crossing cultivated and wild-tolerant tomato accessions (**Fig. 6**). We investigated root system architecture of F1 individuals along with their parental lines and wild sensitive accession, under non-stress and salt stress conditions (**Fig. 6 and Fig. S4**). While no significant differences were observed in the main root growth rate between the examined accessions under control conditions (**Fig. 6B**), F1 displayed a significant increase in main root growth rate under the salt stress compared to the other three genotypes, especially when compared to both wild tomatoes (**Fig. 6B**). F1

and cultivated tomatoes showed an increase in lateral root growth rate compared to two wild tomatoes under control conditions (**Fig. 6C**). Under salt stress, F1 individuals exhibited a remarkable increase in lateral root growth rate compared to all other accessions (**Fig. 6C**). Regarding increase in lateral root number, F1 and wild-tolerant accession exhibited higher rate of lateral root emergence compared to cultivated and wild-sensitive accessions under control condition (**Fig. 6D**), while no significant differences were observed for absolute emergence rates under salt stress (**Fig. 6D**). To investigate how salt stress impacted various aspects of root architecture, we calculated the STI for main root growth, lateral root elongation, and increased lateral root number (**Fig. 6E-G**). F1 showed the highest STI for main root and lateral root growth rates, compared to its parental lines, indicating a synergistic interaction on these phenotypes. On the other hand, F1 inherited the STI for lateral root emergence, similar to wild tomatoes. We further evaluated F1 along with their parental lines for Na^+ and K^+ accumulation and observed that F1 seedlings maintained a low Na^+/K^+ ratio in the root and shoot, similar to the cultivated tomato (**Fig. 6H, Fig. S4**). Together, these results indicate that the salt tolerance traits, including maintenance of lateral root development and sodium exclusion, are dominant traits inherited from the tolerant parent. Additionally, F1 displays synergistic effect (hybrid vigor) for main and lateral root growth rates.

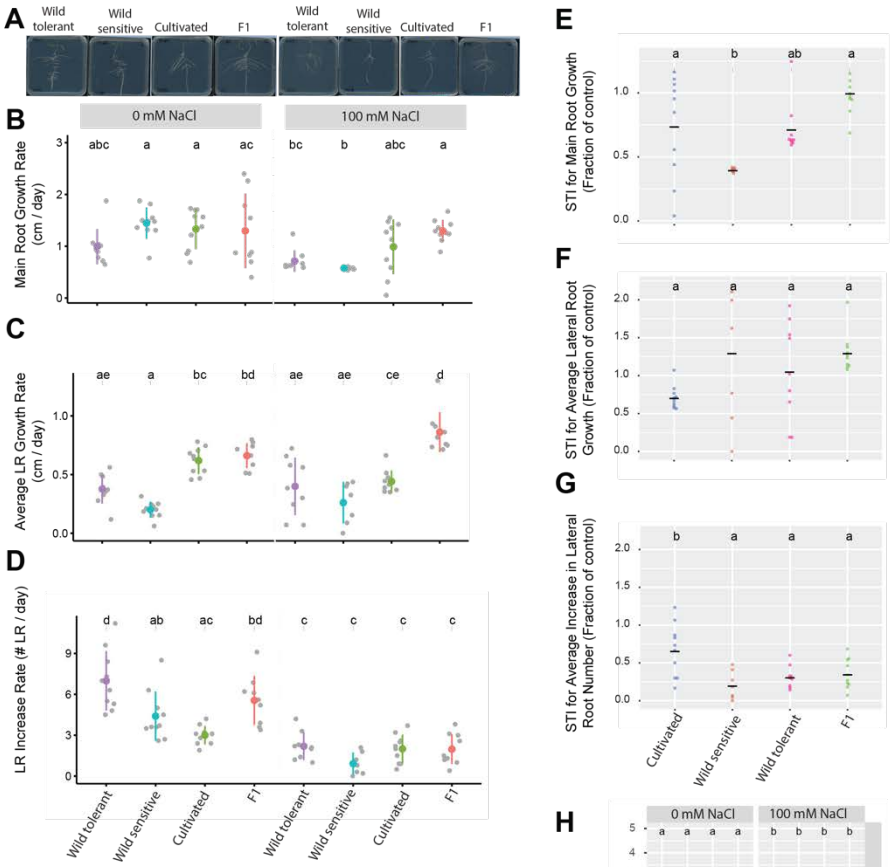

Figure 6. F1 individuals display an increase in main root growth under salt while maintaining lower Na+/K+ ratio in root and shoot. Root system architecture of F1 individuals, their corresponding parents, i.e., cultivated and wild tolerant tomatoes along with wild sensitive tomatoes were investigated with and without 100 mM NaCl. **(A)** Shown are representative images of 9-day-old seedlings that experienced 5 days of salt treatment. Growth rate for **(B)** main root length, **(C)** lateral root length, and **(D)** lateral root number. Salt tolerance indexes (STIs) are shown for the **(E)** main root, **(F)** average lateral root length, and **(G)** lateral root number. The STI was calculated by dividing the growth rate measured under salt stress by the growth rate measured under control condition for each accession. **(H)** Na^+/K^+ ratio of root and shoot of different accessions after 10 days on treatment plates. Each dot represents individual replicas per accession. Statistical analysis was done by comparison of the means for all pairs using Tukey HSD test in all graphs. Levels not connected by the same letter are significantly different ($P < 0.05$).

Segregating F2 population reveals loci on chromosomes 3, 6 and 9 to be associated with lateral root development.

To identify genomic regions associated with the root system architectural traits under salt stress, we generated the F2 population. We investigated the root system architecture of 180 F2 individuals alongside their parental lines under salt stress and identified four phenotypic sub-populations that segregated into four classes regarding their lateral root phenotypes (**Fig. 7A**). The classes comprised individuals with low lateral root length/low lateral root number (low LRL/low LR.no), high lateral root

length/low lateral root number (high LRL/low LR.no), low lateral root length/high lateral root number (low LRL/high LR.no), and high lateral root length/ high lateral root number (high LRL/high LR.no). We pooled 25 seedlings from each sub-population, extracted DNA, and performed whole-genome sequencing in the pools and their two parents for Bulk Segregant Analysis (BSA).

We have performed multiple bulk comparisons to identify genomic regions showing the most variation (**Fig. 7B and Fig. S5**). We found significant associations on chromosomes 3 and 6 with lateral root elongation (high LR.no/low LRL vs. low LR.no/high LRL, **Fig. 7B**) and chromosome 9 with lateral root emergence (low LR.no/high LRL vs. high LR.no/high LRL, **Fig. 7B**). Similarly, we observed a region towards the end of chromosome 9 and chromosome 3 associated with overall lateral root development under salt stress (high LR.no/low LRL vs. high LR.no/high LRL, **Fig. 7B**). These results suggest that the genes positioned on chromosomes 3, 6 and 9 are contributing to the differences in lateral root development between LA2540 and LA1511.

We overlaid the results from BSA and GWAS to narrow down the selection of candidate genes within the identified genetic regions. We identified nine overlapping loci, and 22 gene coding regions that are putatively associated with lateral root development under salt stress (**Table 1, Table S3**). The candidate genes included: two ABC transporter family member genes (*Spim03g102820* and

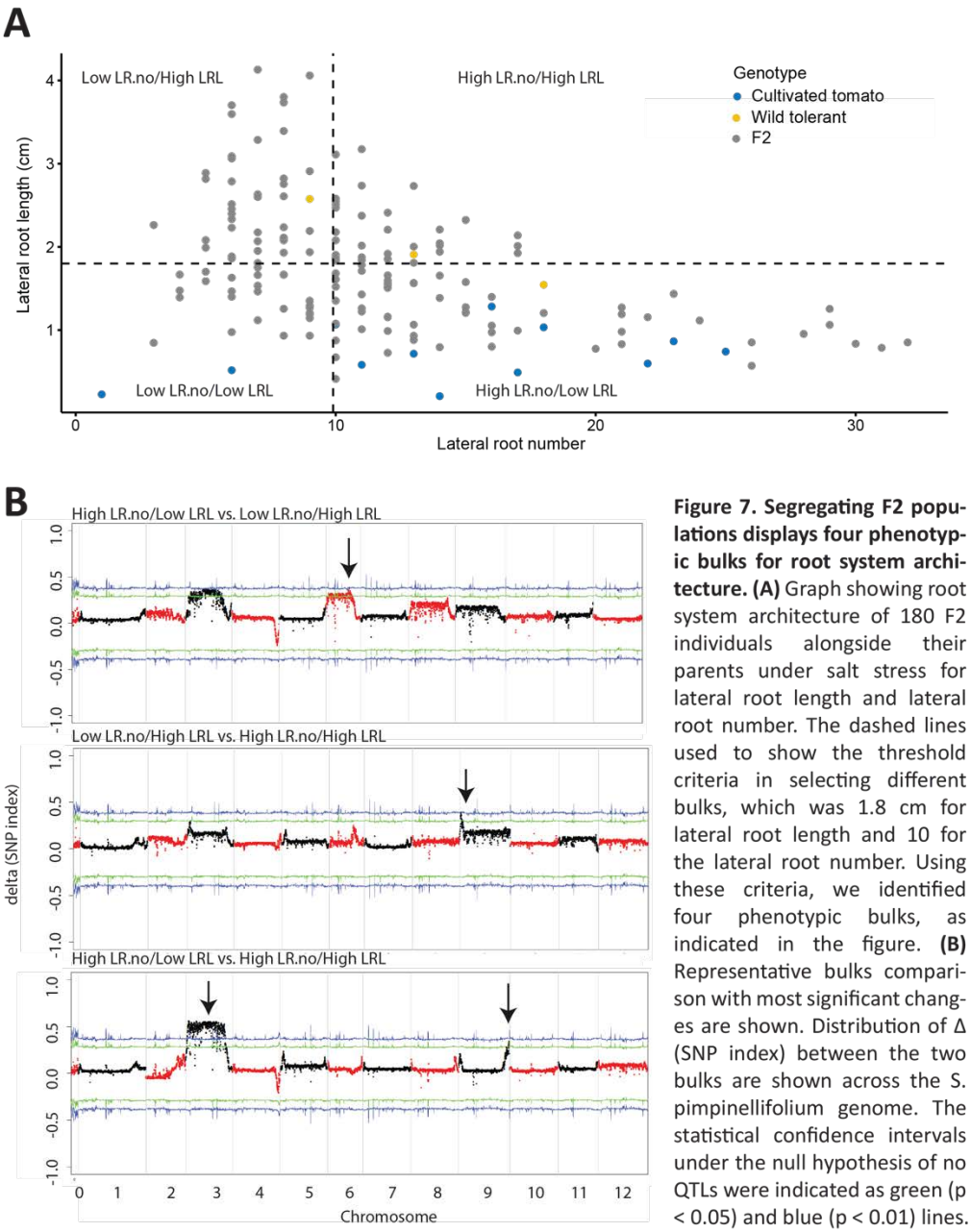

Figure 7. Segregating F2 populations displays four phenotypic bulks for root system architecture. (A) Graph showing root system architecture of 180 F2 individuals alongside their parents under salt stress for lateral root length and lateral root number. The dashed lines used to show the threshold criteria in selecting different bulks, which was 1.8 cm for lateral root length and 10 for the lateral root number. Using these criteria, we identified four phenotypic bulks, as indicated in the figure. **(B)** Representative bulks comparison with most significant changes are shown. Distribution of Δ (SNP index) between the two bulks are shown across the S. pimpinellifolium genome. The statistical confidence intervals under the null hypothesis of no QTLs were indicated as green ($p < 0.05$) and blue ($p < 0.01$) lines.

Spim05g145990), associated with the maintenance of main root length and total root system (MRLpTRS.D1&D2. SALT and TRS.D4.SALT.01); two N-acetylglucosaminyltransferase family genes (*Spim03g108680* and *Spim05g145980*) associated with the average lateral root length and total root system (aLRL.D1.SALT and TRS.D4.SALT); transcription factor bHLH87-like (*Spim03g110510*) and AP2-like ethylene-responsive transcription factor TOE3 (*Spim09g252830*), associated with the maintenance of average lateral root length and main root length per total root system (aLRL.D1.SALT and MRLpTRS.D3&D4.SALT). Additionally, we identified genes involved in the regulation of cellular processes such as those encoding a mannan synthase (*Spim09g253730*), a carboxypeptidase (*Spim09g253210*), a subtilisin-like protease (*Spim06g186120*), and a 3'-5' exonuclease domain-containing protein (*Spim03g110520*), associated with maintenance of main root length and average lateral root length per total root system (MRLpTRS.D4.SALT, aLRLpTRS.D2.SALT, and aLRL.D1.SALT). The L-ascorbate peroxidase gene (*Spim09g252840*) was associated with maintaining the main root length per total root system (MRLpTRS.D3&D4.SALT). Additionally, we identified genes encoding two kinases and three proteins of unknown function, including one containing a domain of unknown function (DUF1677, *Spim06g186130*), which were associated with maintaining either lateral root or main root length per total root system (aLRLpTRS.D2.SALT). Although variation within the natural diversity panel is not guaranteed to be captured within bulk-segregant analysis due to differences in allele frequencies and causal genes; we have identified overlapping genetic elements contributing to root development under salt stress between GWAS and bulk-segregant analysis.

Table 1. List of 22 genes identified by cross-referencing GWAS and BSA analysis. If no genes were found within the chromosome regions indicated by the GWAS, we extended the search by 10 kb before and after the original SNP locations.

Locus	1st SNP	Last SNP	Gene ID	Chromosome	Start	End	Strand	Description
MRLpTRS.D1&D2.SALT	58311594	58318648	Spim03g102820	Chr03	58317465	58333842	-	ABC transporter A family member 7-like
aLRL.D1.SALT	62872139	62872729	no candidate					
+/-10k	62862139	62882729	Spim03g108680	Chr03	62862616	62865458	-	Core-2/I-branching beta-1,6-N-acetylglucosaminyltransferase family
			Spim03g108690	Chr03	62868995	62871907	-	AP-3 complex subunit delta
			Spim03g108700	Chr03	62873276	62881576	-	Histidine--tRNA ligase
aLRL.D1.SALT	64342558	64343225	no candidate					
+/-10k	64332558	64353225	Spim03g110510	Chr03	64340070	64341212	-	Transcription factor bHLH87-like
			Spim03g110520	Chr03	64348724	64354128	-	3'-5' exonuclease domain-containing protein
TRS.D4.SALT	2853323	2873370	Spim05g145980	Chr05	2855866	2859416	-	Core-2/I-branching beta-1,6-N-acetylglucosaminyltransferase family
			Spim05g145990	Chr05	2864524	2873811	+	ABC transporter G family member protein
aLRLpTRS.D2.SALT	39476715	39476898	no candidate					
+/-10k	39466715	39486898	Spim06g186100	Chr06	39466736	39467116	-	Receptor-type tyrosine-protein like
			Spim06g186110	Chr06	39470274	39473093	+	Ring-box protein 1a
			Spim06g186120	Chr06	39473899	39476229	-	subtilisin-like protease
			Spim06g186130	Chr06	39481301	39481819	-	Protein of unknown function (DUF1677)
MRLpTRS.D3&D4.SALT	893689	899226	no candidate					
-10k/+10k	883689	909226	Spim09g252830	Chr09	885469	888212	+	AP2-like ethylene-responsive transcription factor TOE3
			Spim09g252840	Chr09	893083	897835	+	L-ascorbate peroxidase
			Spim09g252850	Chr09	901262	910459	+	Kinase
MRLpTRS.D3&D4.SALT	1235817	1235817	no candidate					
-10k/+10k			Spim09g253200	Chr09	1239184	1244087	+	DnaJ protein like
			Spim09g253210	Chr09	1244798	1246201	+	Carboxypeptidase
MRLpTRS.D3&D4.SALT	1278892	1308283	Spim09g253260	Chr09	1289015	1294003	+	TIR domain-containing protein
			Spim09g253270	Chr09	1304169	1306382	+	Protein kinase domain-containing protein
MRLpTRS.D4.SALT	1688182	1701564	Spim09g253720	Chr09	1691928	1693028	+	Unknown protein
			Spim09g253730	Chr09	1694719	1698430	-	Mannan synthase
			Spim09g253740	Chr09	1699511	1699663	+	Unknown protein

Identification of transcriptional patterns underlying differences in lateral root development under salt stress.

To identify key time points at which WT and CT differ in their lateral root development in response to salt stress, we imaged the development of their root architecture under control and salt stress conditions at 60-minute intervals using SPIRO setup [32](**Fig. 8**). We observed that salt stress exposure immediately reduces lateral root length in CT, while no significant differences in individual lateral root length were observed in WT (**Fig. 8A**). Significant decrease in individual lateral root growth rate was observed from 1,200 minutes after stress exposure onwards in CT (**Fig. 8B**). On the other hand, there was no evident difference in lateral root growth rate of WT until 5,000 minutes after stress exposure, after which salt

exposed lateral roots showed an increased growth rate (**Fig. 8B**). CT developed new lateral roots throughout the experiment under both control and salt stress conditions, albeit at the reduced rate, thereby reducing the average emergence time from 3519 to 4488 minutes after stress exposure (**Fig. 8C**). Although the average emergence time in WT showed even smaller difference between control and salt stress conditions (2841 and 3173 minutes after stress exposure respectively), we did observe a clear delay in lateral root emergence of WT under salt stress compared to the control condition, with no lateral roots emerging until 2,000 minutes after stress exposure (**Fig. 8C**).

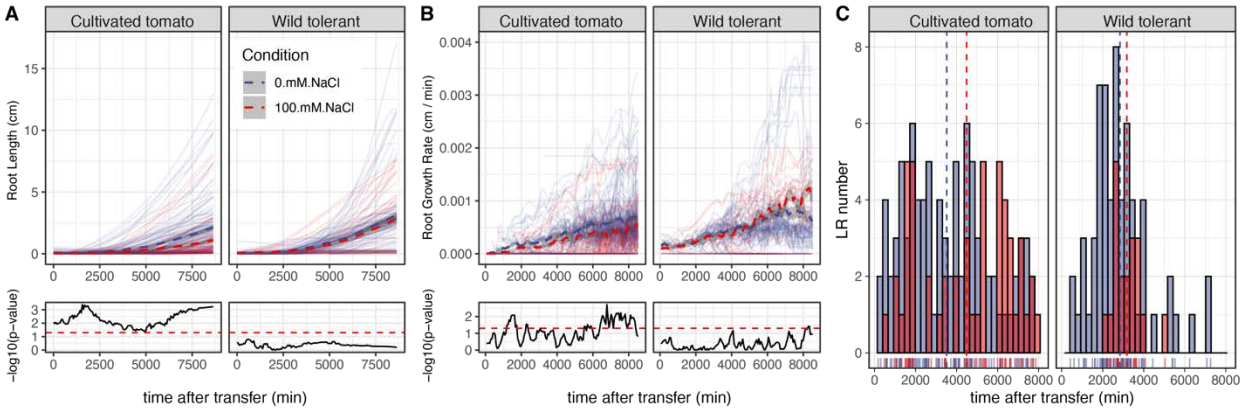

Figure 8. Wild tolerant and cultivated tomatoes show variation in lateral root elongation and emergence under the salt stress. (A) Lateral root length, **(B)** lateral root length growth rate, and **(C)** lateral root number are shown for the two tomato accessions grown in agar plate under 100 mM NaCl. The plates were imaged using SPIRO setup at a 30-min interval for one week. Individual transparent lines indicate the growth trajectory of individual lateral roots, dashed line indicates the growth average per genotype per condition, whereas the shaded area indicates the standard deviation. The differences between Control and Salt conditions were tested within each genotype using one-way ANOVA, with *, ** and *** representing p-values below 0.05, 0.01 and 0.001, respectively. The growth dynamics of lateral roots were measured over two experimental replicates for 4 biological replicates per genotype per condition.

Guided by the time points at which we observed significant differences in lateral root growth and emergence, we performed RNA-Seq analysis of the transcriptional profiles of both CT and WT roots collected at 500, 1000, 2000, 3000, and 4000 minutes after salt stress exposure (**Fig. 9, Table S4**). We identified 3,792 differentially expressed genes (DEGs) in WT (2,261 upregulated and 1,531 downregulated) and 4,032 DEGs in CT (2,307 upregulated and 1,725 downregulated) (**Fig. 9A**). Among these changes, we found 1,467 genes as being upregulated in both accessions while 1,009 genes downregulated. To identify genotype-specific DEGs at specific time points, we compared DEGs across individual time points (**Fig. 9B**). WT showed highest DEGs at 500 min after salt stress exposure (1,796 genes with fold change ≥ 2-fold and adjusted p-value > 0.05), followed by 4,000 min (1,631) (**Table S5**). On the other hand, CT showed the highest number of DEG at 4000 min (2,018 genes with fold change ≥ 2-fold and adjusted p-value > 0.05), followed by 500 (1,989). While both accessions showed the most changes in transcript abundances during early and late time exposure to salt stress, both had the least changes at 3,000 min after salt exposure. To compare the overlap between time points, we generated UpSet plots (**Fig. 9C, Fig. S6**). The analysis revealed that most upregulated DEGs in each accession were detected at 4,000 minutes, while most downregulated DEGs occurred at 500 minutes (**Fig. 9C**). Additionally, we observed that the majority of DEGs in each accession are unique to one or two time points, with only a few DEGs commonly expressed across all time points. Using Go Enrichment Analysis, we looked at which biological process they were involved in. Most DEGs at 500 minutes after salt exposure were enriched with genes involved in stress responses and metabolic processes in WT, or detoxification and transporter activities in CT. Interestingly, at 4,000 minutes, the WT DEGs remained enriched with genes involved in stress responses and metabolic processes, similar to the early response to stress. In contrast, DEGs found in CT showed significant enrichment with genes related to light response, regulatory functions in photosynthesis and cellular binding activities (**Fig. 9C, Table S6**).

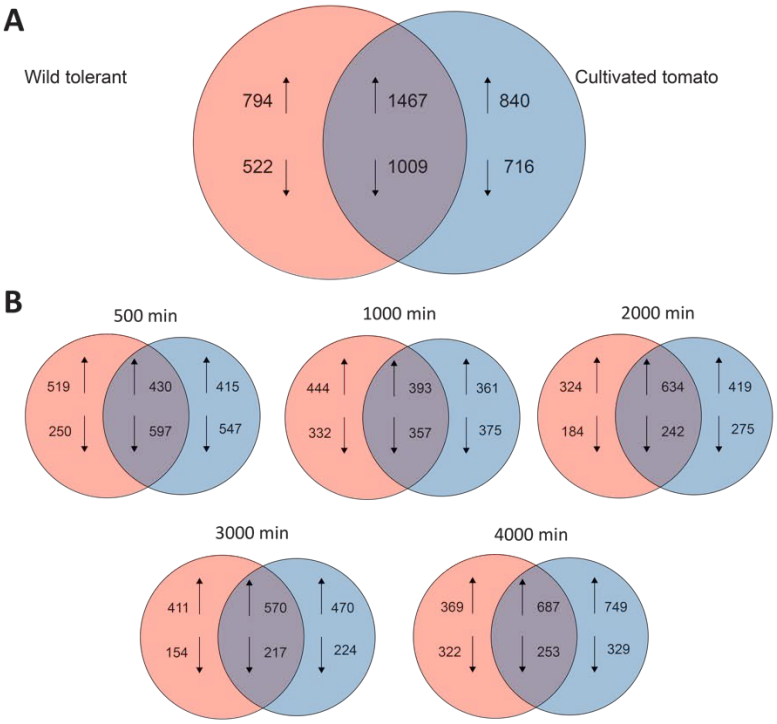

Figure 9. Differentially expression analyses showing unique and common changes in transcriptome of the two tomato accessions in response to the salt stress. (A) Venn diagrams showing number of differentially expressed genes between the two accessions for all timepoints, and **(B)** across individual time points. **(C)** Intersection of numbers of DEGs under salt treatment relative to control condition across five timepoints. The graphs with orange dots represent DEGs in wild tolerant samples and graphs with blue dots represents cultivated tomato samples. The direction of arrow within each panel represents whether DEGs are significantly up- or down-regulated.

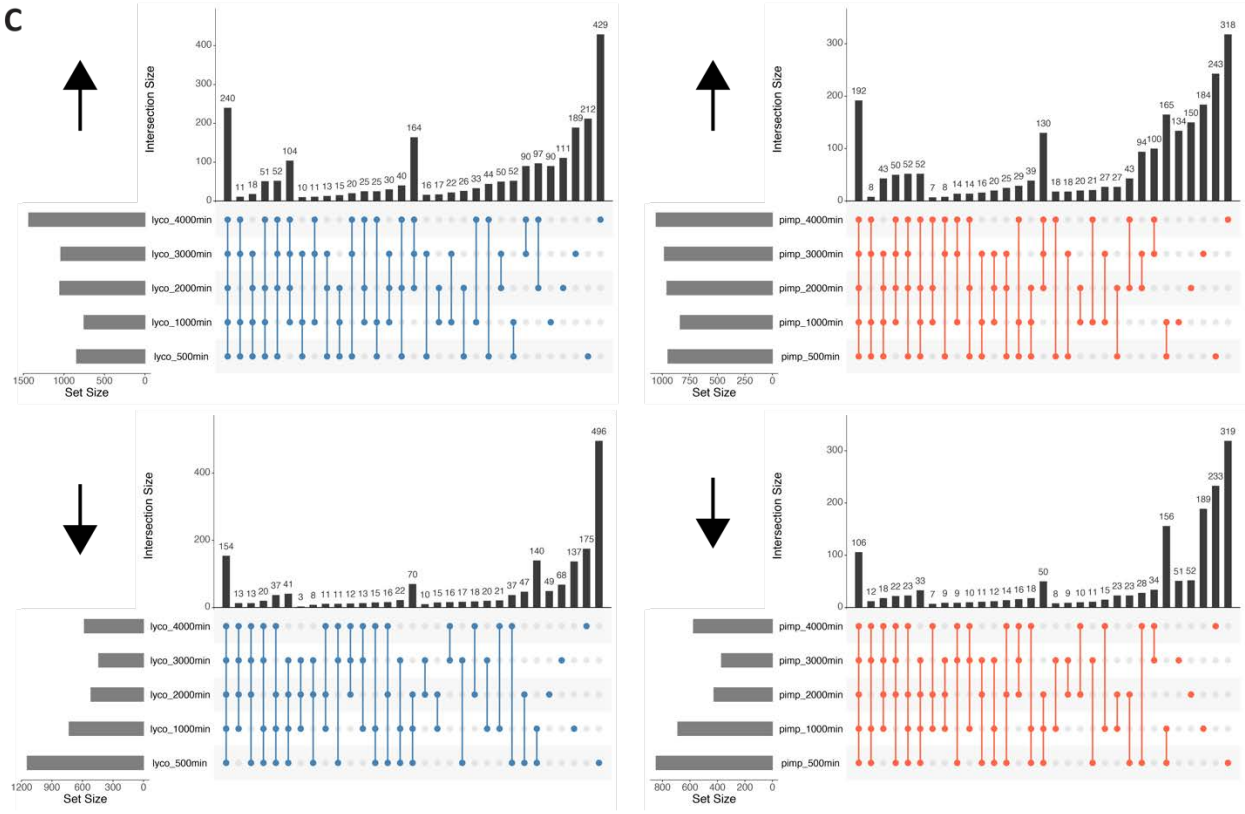

To identify patterns in transcriptional landscape dynamics that putatively underlie the differences in lateral root development between the two accessions, we deployed weighted gene correlation network analysis (WGCNA) [33] and identified 14 gene co-expression modules (**Fig. 10, Fig. S7**). We primarily focused on modules containing our GWAS and/or BSA candidates and those whose expression patterns coincide with the onset of contrasting salt responses of two genotypes. Yellow module (**Fig. 10A**) contained 2,697 genes with repressed expression starting from 1000 minutes after stress exposure in both CT and WT. This reduction in gene expression became more pronounced as the stress persisted, with CT displaying a further decline in gene expression towards the end of the experiment. This module contained one of the genes identified through previous genetic analysis (**Table 1**), encoding an ABC transporter G family member protein (*Spim05g145990*). ABC transporters facilitate the movement of diverse molecules such as organic acids, metal ions, phytohormones, and secondary metabolites, highlighting the importance of cellular transport systems in regulating lateral root development under salt stress.

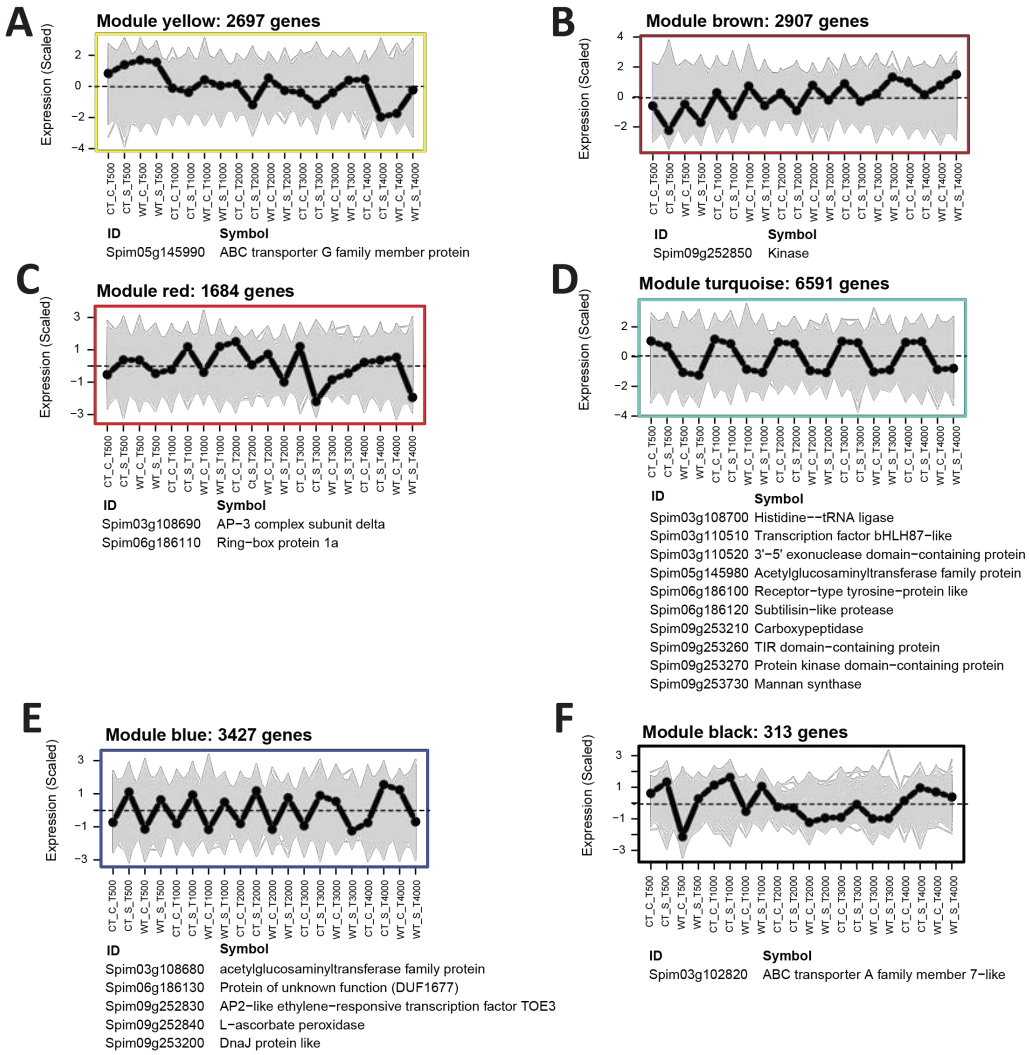

Figure 10. Co-expression network analysis showing distinct patterns among the two accessions across various developmental scales. (A-F) WGCNA co-expression modules with scaled expression values (y axis) across different time points (x axis). Black dotted line indicates eigengene expression profile. Gray line indicates expression values of all genes within the module. Most genes in these modules were positively correlated to the eigengene. Genes that are identified through GWAS and BSA (Table 1) and showing significant association with each module were highlighted below their respective modules. See Figure S5 for a detailed analysis of all 14 modules.

The brown module, comprising 2,907 genes, represented a pattern where gene expression was initially repressed in CT exposed to salt stress, with the gradual recovery of gene expression throughout the salt stress exposure (**Fig. 10B**). Interestingly, WT exhibited a similar repression in the early timepoints (500 to 2,000 minutes post stress exposure), with a more pronounced resurgence at later time points (3,000 and 4,000 minutes post stress exposure). This module contained kinase-like gene (*Spim09g252850*)

previously identified through both GWAS and BSA methods (**Table 1**), indicating its potential role in regulating lateral root development under salt stress.

The red module, comprising 1,684 genes (**Fig. 10C**), represented the genes with increased expression in CT and repressed expression in WT at 500 min. By 3,000 min, expression of genes in the red module was repressed in CT exposed to salt stress, while it continued to increase in WT. Two red cluster genes overlapped with previously identified candidate genes through GWAS and BSA: AP-3 complex subunit delta (*Spim03g108690*) and Ring-box protein 1a (*Spim06g186110*) (**Table 1**). These genes are potentially involved in protein trafficking [34] and protein-protein interaction [35], implying the importance of protein homeostasis during lateral root development.

The turquoise module, comprising 6,591 genes (**Fig. 10D**), was predominantly expressed in CT under both control and salt stress conditions, as compared to WT. This module contained ten genes previously identified through both GWAS and BSA (**Table 1**), including histidine-tRNA ligase (*Spim03g108700*), transcription factor bHLH87-like (*Spim03g110510*), 3'-5' exonuclease domain-containing protein (*Spim03g110520*), core-2/I-branching beta-1,6-N-acetylglucosaminyltransferase family protein (*Spim05g145980*), receptor-type tyrosine-protein like (*Spim06g186100*), subtilisin-like protease (*Spim06g186120*), carboxypeptidase (*Spim09g253210*), TIR domain-containing protein (*Spim09g253260*), protein kinase domain-containing protein (*Spim09g253270*), and mannan synthase (*Spim09g253730*). These genes contribute to maintaining cellular function through various processes, including protein homeostasis, signaling, and structural integrity.

The blue module, comprising 3,427 genes (**Fig. 10E**), was upregulated in response to salt stress in CT at all time points. Genes in the blue module exhibited a similar salt-specific upregulation pattern in WT from 500 min to 2000 min but were repressed at later time points. Five genes from **Table 1** were found in this module, including core-2/I-branching beta-1,6-N-acetylglucosaminyltransferase family protein (*Spim03g108680*), protein of unknown function (DUF1677) (*Spim06g186130*), AP2-like ethylene-responsive transcription factor TOE3 (*Spim09g252830*), L-ascorbate peroxidase (*Spim09g252840*), and DnaJ protein like (*Spim09g253200*). These genes are involved in maintaining cellular function through processes such as protein modification, stress response, regulation of gene expression, protection against oxidative damage, and proper protein folding.

The black module consisted of 313 genes (**Fig. 10F**) that were upregulated during the early onset of salt stress in both WT and CT, but little difference between treatments at later time points. One of the black module genes overlapped with previously identified candidate genes (**Table 1**), encoding the ABC transporter A family member 7-like (*Spim03g102820*), suggesting the importance of cellular transport systems in regulating lateral root development under salt stress. Together, these findings suggest that the differences in lateral root development under salt stress rely on genes expressed either in the initial phase of salt stress exposure (e.g., yellow module) or are constitutively different in their expression between CT and WT (e.g., turquoise and blue modules).

Identification of most promising candidate genes underlying lateral root development under salt stress. To identify which of the 22 genes (**Table 1**) showed changes in gene expression during the captured developmental time frame, we cross-referenced these 22 genes with RNA-Seq data from root transcriptomics profiles. While all 22 genes displayed some degree of expression across various time points and samples (**Table S4, Fig. S8**), only four candidate genes exhibited significant changes in gene expression in response to salt stress, either in both or one accession, across different time points (**Fig. 11A**). These four genes encoded a protein of unknown function (DUF1677, *Spim06g186130*), an AP2-like ethylene-responsive transcription factor TOE3 (*Spim09g252830*), a L-ascorbate peroxidase (*Spim09g252840*), and an unknown protein (*Spim09g253720*). Both DUF1677 and ethylene-responsive transcription factor TOE3 exhibited transcriptional repression upon exposure to salt stress in both CT and WT, followed by a transcriptional recovery and another decrease, indicating the significance of their

suppression for salt stress response. The transcripts of L-ascorbate peroxidase showed a significant increase in expression throughout the experiments in CT, but this pattern was much more transient in WT. This suggests the importance of L-ascorbate peroxidase expression for lateral root development under salt stress conditions; however, we cannot distinguish whether it acts on lateral root elongation or emergence. The transcripts of the unknown protein increased exclusively in WT during early timepoints, but not in CT, suggesting the importance of dynamic expression of this gene across various developmental stages.

To investigate the allelic variation responsible for differences in gene expression and function, we compared CT and WT for the four best candidate genes using the Integrative Genomics Viewer (IGV) (https://igv.org/)(**Fig. 11B**). Distinct SNPs were detected in the 5' UTR, 3' UTR, and intronic regions of both CT and WT, indicating their possible roles in modulating transcription and mRNA stability. Only two missense SNPs were identified within the coding sequences of DUF1677 and the AP2-like ethylene-responsive transcription factor TOE3. In both cases, the CT exhibited an SNP variant from the reference *S. pimpinellifolium LA2093* genome [36], where a C was changed into a T, occurring in the only exon of DUF1677 (changing Proline (CCC) to Leucine (CTC)) and the ninth exon of the ethylene-responsive transcription factor (changing Alanine (GCT) to Valine (GTT) or Leucin (CTT) to Phenylalanine (TTT)). Overall, the coding sequences appears to be conserved between the two accessions. These results suggest that potential variants causal to associations with these genes are present in gene regulatory sequences, resulting in modulation of gene expression and mRNA stability.

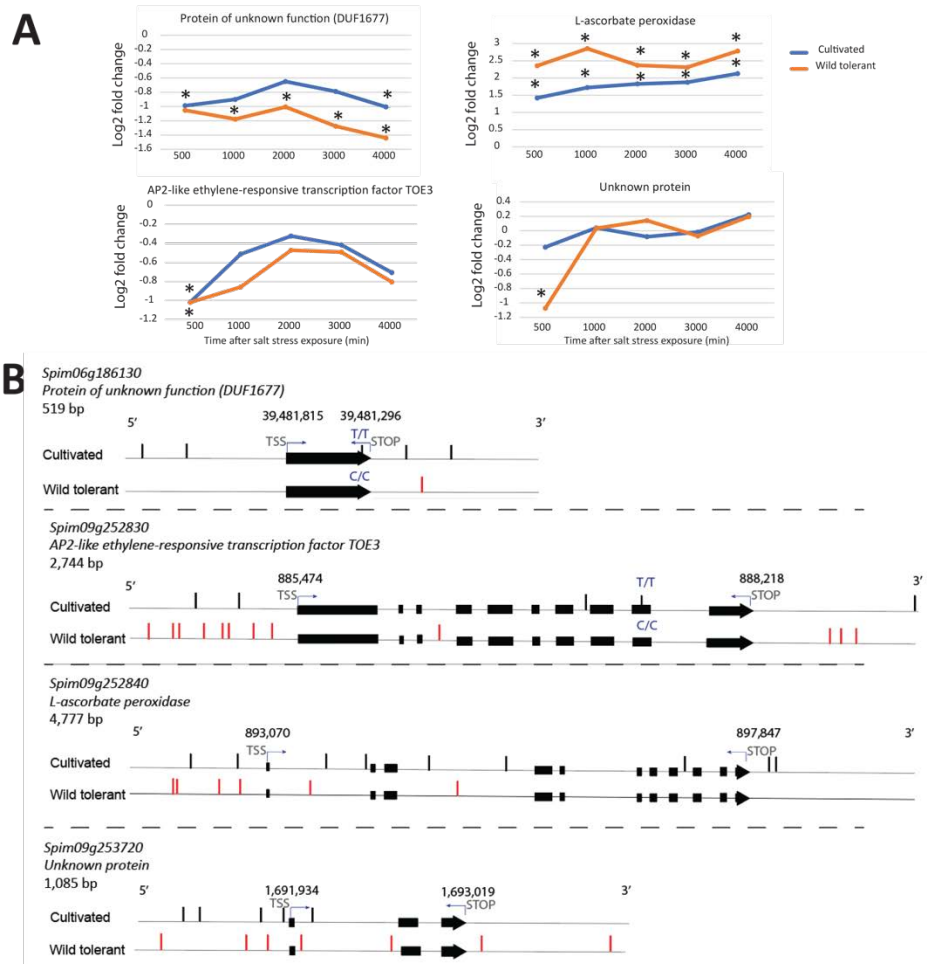

Figure 11. Allelic variants analysis revealed the two accessions are almost conserved in their coding sequence but not in the intronic region, as well as 5' and 3' UTRs. (A) Log2 fold changes are shown for the four genes identified by cross-referencing the three experiments, GWAS, BSA, and RNA-Seq, across all developmental time points for the two accessions. Stars indicate statistically significant changes in gene expression, defined as a fold change of ≥ 2 and an adjusted p-value of < 0.05. **(B)** Gene models are illustrated for the four genes, with unique SNP positions depicted as straight lines. The positions of the transcription start site (TSS) and STOP are indicated, with gene locations displayed above. SNPs resulting in missense mutations are depicted along with their corresponding variants in the other accession. See Table S3 for the comprehensive list of variant analyses conducted for the 22 genes identified from GWAS and BSA analyses (Table 1).

Discussion

Harnessing the inherent genetic diversity found in wild relatives, traditional landraces, and modern cultivars is essential for ensuring food security, a critical priority for crop enhancement initiatives. Genetic diversity within the wild progenitors of our cultivated crop species has been largely recognized as an important resource for increasing climate resilience of modern-day agriculture [12,37]. In tomato, GWAS has been used for detecting genetic variations underlying complex agronomic and morphological traits [38–43]. Although various components of salinity tolerance have been identified in S. pimpinellifolium [12,28,29], this is the first study that explores root system architecture-derived mechanisms of salt tolerance.

We have used a previously developed natural diversity panel of 220 diverse wild tomato accessions to identify alleles associated with root system responses to salt stress. A total of 191 significant associations corresponding to 55 genetic loci have been identified, of which nine showed overlap with BSA and RNA-seq studies. Moreover, we have identified accession LA2540 (WT) to be salt tolerant, which interestingly was identified as one of the more resilient S. pimpinellifolium accessions in field and greenhouse-based studies [12]. Unlike in Arabidopsis, where natural variation in salt-induced changes in root architecture resides in both main and lateral roots [44], we have identified that salt-induced changes in S. pimpinellifolium root architecture are associated with differences in lateral root development (Fig. 1, Fig.2). Initially, we investigated the differences between salt tolerant and sensitive accessions of S. pimpinellifolium (Fig. 5). However, we have identified a more interesting pattern of salt stress response in a cultivated tomato, LA1511 (CT), that showed complementary response in its lateral root development to LA2540 (WT), the wild tolerant tomato (Fig. 5). Through generation of F1 hybrids between WT and CT, we have determined that the lateral root traits of both cultivated and wild tolerant accessions can be combined and act on complementary aspects of salinity tolerance. F1 hybrid exhibited an increase in STI for average lateral root length when compared to each parent (Fig.6F). Additionally, F1 maintained a lower Na^+/K^+ ratio, mimicking the cultivated parent and prioritizing tolerance by exclusion of sodium in the shoot (Fig. 6H) [45]. Together, these findings suggest that combining the complementary strategies of salinity tolerance, based on complementary characteristics of lateral root development, results in increased resilience of F1 hybrids.

Bulk-segregant analysis (BSA) detected three genomic regions harboring potential gene candidates responsible for the root system maintenance under the salt. Overlaying BSA with the GWAS result, we identified 22 gene candidates (Table 1). The fact that only four out of 22 genes showed a significant change in the transcript abundances under salt stress (Fig. 11, Fig. S7) does not preclude the importance of these genes, which may be attributed to their transcription not being responsive within the sampling window of our RNA-Seq experiments or they are regulated at post-transcriptional level. The observation that 17 of these genes cluster into shared co-expression network modules (Fig. 10), encompassing the red module with two genes, the turquoise module with 10 genes, and blue module with five genes, implies they exhibit similar expression profiles across comparable conditions or samples, hinting at potential functional associations or co-regulation among these genes.

The turquoise module includes genes associated with cellular homeostasis and maintenance, such as those encoding carboxypeptidase (Spim09g253210) and mannan synthase (Spim09g253730), involved in cell wall homeostasis, along with subtilisin-like protease (Spim06g186120) and 3'-5' exonuclease domain-containing protein (Spim03g110520), implicated in protein and DNA quality control. Plant subtilases are characterized by glycosylation, a post-translational modification regulating their activity. In Arabidopsis, subtilase AIRS gene promoter is active at sites of lateral root emergence, suggesting its role in digesting structural proteins within the extracellular matrix, facilitating lateral root emergence [46]. Our findings indicate that the expression of subtilisin-like protease and mannan synthase genes is repressed throughout the observed period (Fig. S7). Notably, while the repression of mannan synthase continued as stress progressed, the expression of subtilisin-like protease began to increase toward the end of the

observed period. This differential expression suggests distinct regulatory mechanisms of lateral root development responses to salt stress. Understanding these processes provides insights into the complex regulation of gene expression during lateral root emergence under salt stress conditions.

Both L-ascorbate peroxidase (Spim09g252840) and AP2-like ethylene-responsive transcription factor TOE3 (Spim09g252830) were contained in the blue co-expression module (Fig. 10), show significant changes in transcript abundances in response to salt stress (Fig. 11), and are located within similar genomic regions (Table 1, chromosome 9). These observations confirm the initial association of these two genes with their role in lateral root development under salt stress. Salinity stress leads to oxidative stress and cellular damage. The antioxidant system mitigates oxidative damage by counteracting the generation of reactive oxygen species (ROS) [47,48]. Salt tolerance is positively correlated with the cell's antioxidant capacity [45,48–53], additionally supported here by an increase in the expression of ascorbate peroxidase throughout our experiment (Fig. 11). The consistent expression of ascorbate peroxidase can be explained by two potential mechanisms. First, the initial reactive oxygen species (ROS) generated by salt stress trigger root cells to enhance their antioxidant response. Second, the emergence of lateral roots requires cell rupture, which generates another wave of ROS signal in a localized area of the root environment, further amplifying the increase in transcript levels. These potential mechanisms highlight the complex interplay between stress responses and root development.

Similar to other ethylene-responsive transcription factors, the AP2-like ethylene-responsive transcription factor TOE3 likely regulates gene expression in response to ethylene. The impact of ethylene on salt stress varies greatly across species and developmental stages, acting as a double-edged sword. While it enhances salt tolerance in Arabidopsis, it has also been reported to have negative effect in rice. Ethylene signaling mutants in Arabidopsis (ein3 eil1 double mutants) show reduced salt tolerance, whereas RNAi transgenic rice plants (OsEIL1 and OsEIL2) display increased salt tolerance [54–57]. We found that the expression of AP2-like ethylene-responsive transcription factor TOE3 was significantly repressed initially after salt stress exposure in both accessions, but it began to increase during the stress and decreased toward the end of the experiment (Fig. 11). This pattern highlights that different developmental stages in lateral roots require varying levels of ethylene signaling and suggests that the initial repression is necessary for lateral root development under early salt stress exposure.

In conclusion, our integrative approach identifies candidate genes involved in lateral root development under salt stress conditions, providing compelling evidence that ethylene signaling and the antioxidant scavenging system are pivotal factors in regulating lateral root development under salt stress. The data generated in this study will prove invaluable for future functional validation studies aimed at elucidating the precise roles of these genes during early root development in response to salt stress, contributing to the broader objective of enhancing plant productivity under saline conditions.

Materials and Methods

Agar-based plate experiments

Tomato seeds were sterilized for 10 min with 50% bleach and rinsed five times using autoclaved milli-Q water, and germinated on ¼ strength Murashige and Skoog (MS) medium containing 0.5% (w/v) sucrose, 0.1% (w/v) 4-morpholineethanesulfonic acid (MES), and 1% (w/v) agar, with pH adjusted to 5.8 with KOH. After 24 h of vernalization at 4 ˚C in the dark, the plates were placed in the Conviron growth chamber with the light intensity of 130–150 µmol x m^{-2} x s^{-1} in a 20 h light / 4 h dark cycle at 25 ˚C day / 20 ˚C night and 60% humidity. 4 days after germination, the seedlings were transferred to 1/4 MS media with and without 100 mM NaCl, as indicated in the figures. Each plate contained one tomato seedling for root system architecture analysis. The plates were scanned using EPSON scanner every 5 consecutive days, starting from day 4 after germination. To analyze root system architectural traits from the scanned plate images, we used SmartRoot plugin [58] in ImageJ to manually trace the root, and extract root-related features in the CSV format followed by data analysis in R. The root system architecture assays for the initial experiment to evaluate the root system architecture responses of natural diversity panel were conducted over six experimental batches, with four biological replicates per genotype per condition. The quantified data averaged per genotype and condition is listed in Table S1. The original image data, together with the traced files can be found at https://doi.org/10.5061/dryad.nk98sf826. The R-script used to curate and process the raw phenotypic data can be accessed at (https://rpubs.com/mjulkowska/BIGpimp_RSA_salt). The R-notebooks for the analysis of individual follow-up experiments can be accessed at RPubs - 20211201_M248M058LA1511_RSA_analysis, RPubs - 20230502_RSA_F1_100mM_Salt, RPubs - 20230612_F1_FW_DW_ICP_Salt, RPubs - 20230605_RSA_analysis_F2_100mM_Salt_d9_all_batches_final). The data analysis and visualization has been performed using ggplot2, ggpubr, corrplot, ggbeeswarm, ggridges, gapminder, RColorBrewer, ColorRamps, doBy, reshape2, cowplot, plotly and tidyverse libraries [59–69].

Genome wide-association study

The genome wide-association study has been performed using the data from 220 *S. pimpinellifolium* accessions using the ASReml script as described in [12]. Briefly, the SNP data has been curated and imputed for missing and heterozygous SNPs, and ran using three PCA components as estimations for population structure, and kinship matrix calculated using GAPIT [70]. The code used for running the ASReml-based script can be accessed at https://github.com/mmjulkowska/Pimp_RSA_GWAS_salt/blob/main/20211011_RSA_GWAS_prep.R andhttps://github.com/mmjulkowska/Pimp_RSA_GWAS_salt/blob/main/20220101_ASReml_prep_for_pimp_RSA.R. The ASReml-method GWAS output files can be accessed at https://doi.org/10.5061/dryad.nk98sf826. Additionally, we have used the entire SNP dataset to run EMMA X method [31], using 3 PCA components as estimations for population structure, and kinship matrix calculated using the essential SNP set. The code used for running the EMMAX-based script can be accessed at https://github.com/mmjulkowska/Pimp_RSA_GWAS_salt/blob/main/20240208_EMMAX_GWAS%20pipeline.md. The EMMA-X GWAS output files can be accessed at https://doi.org/10.5061/dryad.nk98sf826. The data was subsequently investigated for all SNPs with association p-value above genome-wide threshold of -log10(p-value) > 5, as well as minor allele frequency and overlap of associations across individual traits and neighboring SNPs. The list of strongly associated SNPs can be found in **Table S2**.

Elemental analysis

The elemental analysis was performed using Inductively Coupled Plasma Atomic Emission Spectroscopy (ICP-AES). For analysis of Na^+ and K^+ ions in roots and shoots of plate-grown seedlings, the plants were grown on 1/4 x MS plates as described above. After 10 days of exposure to 0 or 100 mM NaCl, root and shoot tissues were harvested and measured for fresh weight, rinsed in milli-Q water and collected into separate paper bags that were dried at 60 °C for 2-3 days. Subsequently, the dry weight was recorded. Samples were digested in double distilled HNO_3, followed by the addition of 60/40 nitric/perchloric acid (v/v), continuing incubation at 150 °C. Samples were processed for ICP-AES analysis using a Thermo iCap 7000 ICP-AES after being diluted to 10 ml with deionized water. Ion content was calculated per dry weight for each sample, followed by data analysis in R.

Generating the F1 hybrid and screening the F2 population for variation in later root length and number

The F1 hybrid population was created through reciprocal crosses between two tomato varieties: the cultivated tomato (*S. lycopersicum* LA1511) and the wild tolerant tomato (*S. pimpinellifolium* M248). The F1 hybrid underwent self-pollination to produce the F2 segregating population. From this population, 180 F2 tomato seeds were used for Bulk Segregant Analysis (BSA). The seeds underwent processing similar to that described for the agar-based plate experiments mentioned above for screening root system architecture. Following the root system architecture analysis, we identified four distinct bulks within the F2 population based on lateral root length and number. These bulks were then subjected to DNA extraction.

DNA extraction for genome sequencing

From each bulk, we pooled 25 individuals that had the best characteristic of their designated pool for DNA extraction from roots. Extraction of the DNA was carried out using Wizard® Genomic DNA Purification Kit (Promega, catalogue # A1125) according to the manufacturer instructions. The integrity of DNA samples was checked using the electrophoresis gel and the concentration was determined by measuring the absorbance at 260 nm in a Nanodrop. 500 ng/µl of DNA from each pool and the two parents were sent on dry ice to the Novogene (Sacramento, CA, USA) for genome sequencing.

Bulk Segregant Analysis (BSA)

Raw paired-end reads were processed to trim adaptor and low-quality sequences using Trimmomatic (version 0.39) [71]. The processed reads were aligned to the reference *Solanum pimpinellifolium* genome [36]) using BWA-MEM (0.7.17-r1188) [72] with default parameters. Following read mapping, duplicated read pairs in each sample were marked using Picard (v2.26.6; http://broadinstitute.github.io/picard/), and SNPs were then called from the marked alignment files using GATK (v4.1.4.1) [73]. The called SNPs were filtered using GATK with parameters 'QD < 2.0 || FS > 60.0 || MQ <40.0 || MQRankSum < -12.5 || ReadPosRankSum < -8.0'.

For BSA-Seq analysis, in each comparison of two bulks, SNP index of each SNP site was calculated for each bulk by dividing the number of reads harboring the allele of one parent with the total number of reads covering the site. Δ(SNP index) was then calculated by subtracting the SNP index in one bulk from the SNP index in the other bulk. An average Δ(SNP index) in each 200-kb sliding window with a step size of 100 kb across the *S. pimpinellifolium* genome was calculated. The 95% and 99% confidence intervals of the Δ (SNP index) under the null hypothesis of no QTLs were also calculated following the method described in [74]. QTLs were then identified as genomic regions with the Δ (SNP index) larger than the threshold ($p < 0.05$).

Root sample collection for RNA-Seq experiment

To determine the time points corresponding to both pre- and post-lateral root emergence in the presence

and absence of 100 mM salt, we utilized the Smart Plate Imaging Robot (SPIRO) platform to capture images of tomato seedlings cultivated on agar plates at 30-minute intervals over the course of one week. Subsequently, we analyzed these images using SmartRoot, and processed in an R-pipeline that can be accessed at (https://rpubs.com/mjulkowska/tomato_LR_LA1511vsM248) to identify the time points at which lateral roots emerged. Based on this analysis, we selected five time points spanning before, during, and after lateral root emergence under both control and salt stress conditions, specifically at 500, 1000, 2000, 3000, and 4000 minutes after transfer to the treatment plates. Following this selection, we collected root samples, excluding the 0.5 cm root tip, from the two tomato accessions at the designated time points in three independent biological replicates. These samples were promptly frozen in liquid nitrogen and stored at -80°C for subsequent analysis.

RNA isolation, library preparation, and sequencing

Total RNA from roots were extracted using RNeasy Plant Mini Kit (Qiagen, Invitrogen, catalog # 74904), including a cleaning step using RNase-free DNase to eliminate genomic DNA contamination. The integrity and quality of RNA samples were evaluated using the Qubit RNA IQ Assay Kit (ThermoFisher Scientific, catalog # Q33221) and its concentration were evaluated using Qubit RNA HS Assay Kit (ThermoFisher Scientific, catalog # Q32852). 500 ng/µl of total RNA from each sample was sent on dry ice to the Novogene (Sacramento, CA, USA) for library preparation using NEBNext Ultra™ II RNA Kit for Illumina (Catalog# E7770L) paired end x 150 bp unstranded sequencing using NovaSeq. RNA-seq data were processed, in brief, using "trimmomatic" (v0.32, parameter: LEADING:3 TRAILING:3 MINLEN:36, TruSeq3-PE.fa:2:30:10:2, [71]) to remove adaptors and low-quality reads. Then, clean reads derived from *S. pimpinellifolium* and *S. lycopersicum* were mapped to the *S. pimpinellifolium* reference genome by Hisat2 (v2.1.0, parameter: --rna-strandness RF -p 60 --no-softclip, [75]). Afterwards, the BAM files were processed by FeatureCounts to quantify transcript abundance at the gene level (v2.0.1 [76], parameter: -s 1 -p -t mRNA -g ID -O). DESeq2 (v3.19, [77]) was used to normalize read counts among the 60 samples and identify differentially expressed genes (DEGs). Here, we included the four timepoint (500min, 1000min, 2000min, 3000min, 4000min), two species (*S. pimpinellifolium* and *S. lycopersicum*), and treatments (Control and Salt) as the experimental design factors. Then condition-wise DEGs per time points per species were identified using the cutoff of adjusted p-value < 0.05. Intersections of DEGs among time-points and species were characterized by the UpsetR plot function in R [78]. The effect of timepoints, species, and treatment on transcriptome response was examined by principal component analysis (PCA) using in-house R-scripts (https://github.com/Leon-Yu0320/Tomato-salt-stress-transcriptome). Briefly, the PC values were calculated using the top 25% most variable genes based on standard deviation (SD) the PCA plot was visualized with ggplot2 [59].

Go enrichment analysis

GO term enrichment analysis was performed to identify over-represented GO terms in the biological process category using Blast2GO (v3.1.11) [79]. The Fisher's exact test with the FDR correction for multiple testing was used to determine statistical significance (adjusted *P* value < 0.05).

Co-expression network analysis

Co-expression network modules were built with the weighted gene correlation network analysis (WGCNA) R package version 1.72-1 (Langfelder and Horvath, 2008). Normalized counts were used as an input and 75% of the most variable genes were used for analysis. A scale-free network was created by applying a soft threshold power of 5. We created an unsigned network using the blockwiseModules function with following parameters: corType = bicor, max PO utliers = 0.05, merge Cut Height = 0.4 and max Block Size = 25 000. Gene Ontology enrichment analysis was carried out with GoStats R package version 2.62.0 with a

standard hypergeometric test, to evaluate the enrichment of categories in each module compared to the set of all genes used to create the co-expression network.

Data availability

Raw genome sequencing reads from Bulk Segregant Analysis (BSA) and RNA-Seq raw reads have been deposited in the National Center for Biotechnology Information BioProject database under the accession numbers PRJNA1108418 and PRJNA1119579, respectively. The phenotypic data in both raw and processed state, and GWAS results can be accessed at https://doi.org/10.5061/dryad.nk98sf826.

Acknowledgments

The authors would like to thank BTI and KAUST Greenhouse Teams for caring for the plants. The authors would like to acknowledge support from the NSF-IOS #2023310 (ADLN) and NSF-IOS #2102120 (ADLN), NSF Mathematical Biology #2244735 (MMJ). The majority of funding for this work was generously provided by KAUST, with baseline funding awarded to Mark Tester and BTI's startup funds awarded to Magdalena Julkowska.

Author contributions

M.R.I. and M.M.J. conceived the project and wrote the manuscript with inputs from all coauthors, M.M.J. performed GWAS, M.M.J and H.S. quantified the root architecture data for the GWAS population, M.R.I. conducted majority of the experiments including RSA analysis of selected accessions, generation of F1 hybrid and F2 segregating population, RSA analysis of F2 population for bulk segregant analysis, collected samples and extracted DNA for bulk segregant analysis, analyzed ion content data from ICP-AES, M.M.J. and M.R.I. both collected samples for the time-series RNA-Seq experiment, M.R.I. extracted RNA for time-series RNA-Seq experiment, M.P. and E.C. performed ICP-AES, A.D.L.N. and L.Y. performed RNA-Seq DEGs analysis, D.K. performed Co-expression network analysis, Z.F. and X.Z. performed Bulk Segregant analysis and GO enrichment, M.A.T. helped with providing infrastructure for the initial screen and initial funding for the experiments.

Competing interests

The authors declare no competing interests

Correspondence and requests for materials

should be addressed to Dr. Magdalena M. Julkowska (mmj55@cornell.edu).

Figures and tables legend

Table 1. List of 22 genes identified by cross-referencing GWAS and BSA analysis. If no genes were found within the chromosome regions indicated by the GWAS, we extended the search by 10 kb before and after the original SNP locations.

Figure 1. Diversity of salt stress responses observed within the *S. pimpinellifolium* diversity panel. The 220 genotypes of *S. pimpinellifolium* were germinated on ½ MS agar plates for 4 days and subsequently transferred to media containing 0 or 100 mM NaCl (Control and Salt respectively). The seedlings were imaged every 24 h after transfer for 7 consecutive days. The Root Architecture of seedlings was quantified for the first 4 days after transfer, and the **(A)** growth of Main Root, **(B)** increase in Lateral Root number and **(C)** growth of average Lateral Root was estimated using linear growth functions. The population average values for Control and Salt conditions are indicated using the dashed lines. The effect of the treatment was evaluated using a paired Wilcoxon test for **(D)** Main Root Growth Rate, **(E)** increase in Lateral Root number and **(F)** average Lateral Root Growth Rate. The individual gray lines illustrate the genotype-specific change in individual growth parameters across the conditions. **(G)** The genotype-specific growth rates at individual conditions were used to calculate the Stress Tolerance Index (STI) for individual traits, calculated by dividing growth rate estimated under Control / Salt conditions. The relative change in STI represents the salt-induced reprogramming of the root architecture. The individual gray lines represent the genotype-specific change in STI across individual components of root architecture. The individual dots represent the genotype-specific mean calculated from 4 biological replicates.

Figure 2. Salt-induced changes in root biomass distribution between main and lateral roots are associated with loci on Chromosomes 3 and 4. Genome Wide Association Study was performed on 9M SNPs using standard EMMA-X method. Only SNPs with minor allele frequency > 0.05 were used for plotting the Manhattan plot for associations identified with **(A)** ratio of main root length to total root size at 1 day and **(B)** two days post transfer to salt stress, with pseudo-heritability values of 0.116 and 0.195 respectively. The red line indicates the Bonferroni threshold, whereas the blue line indicates genome-wide suggestive threshold. **(C)** The significantly associated loci were inspected in further detail for the gene coding sequences within the regions with significantly associated SNPs. The region on chromosome 3 contained 29 SNPs with -log10(p-value) > 5. The three individual loci **(D-F)** identified on chromosome 4 contained 240, 39 and 85 SNPs with -log10(p-value) > 5. The association graph below each locus represents the association strength with the ratio of main root length to total root size at 1 day after salt stress imposition.

Figure 3. Salt-induced changes in lateral root development are associated with loci on chromosomes 1, 3 and 10. Genome Wide Association Study was performed on 9M SNPs using standard EMMA-X method. Only SNPs with minor allele frequency > 0.05 were used for plotting the Manhattan plot for associations identified with **(A)** average lateral root length and **(B)** lateral root number at one day post transfer to salt stress, with pseudo-heritability values of 0.145 and 0.358 respectively. The red line indicates the Bonferroni threshold, whereas the blue line indicates genome-wide suggestive threshold. **(C)** The significantly associated loci were inspected in further detail for the gene coding sequences within the regions with significantly associated SNPs. The region on chromosome 1 contained 27 SNPs, **(D)** the region on chromosome 3 7 SNPs, and **(E)** region on chromosome 11 contained 60 SNPs with -log10(p-value) > 5. The association graph below each locus represents the association strength with the average lateral root length at 1 day after salt stress imposition.

Figure 4. Emergence of lateral roots and main root growth rate is associated with loci on chromosomes 12 and 22. Genome Wide Association Study was performed on 9M SNPs using standard EMMA-X method. Only SNPs with minor allele frequency > 0.05 were used for plotting the Manhattan plot for associations identified with **(A)** lateral root emergence and **(B)** main root growth rate under salt stress, with pseudo-heritability values of 0.855 and 0.628 respectively. The red line indicates the Bonferroni threshold, whereas the blue line indicates genome-wide suggestive threshold. **(C)** The significantly associated loci were inspected in further detail for the gene coding sequences within the regions with significantly associated SNPs. The region on chromosome 12 contained 16 SNPs, whereas **(D)** the region on chromosome 11 contained 15 SNPs -log10(p-value) > 5. The association graph below each locus represents the association strength with the trait initially associated with that locus.

Figure 5. Wild tolerant and cultivated tomatoes have different salt tolerant features regarding lateral root development under the salt. (A-C) Root system architecture analysis of cultivated and wild tomatoes under 0 or 100 mM concentrations of NaCl are shown**. (D)** Salt tolerance indexes (STIs) are shown for the main root, **(E)** average lateral root length, **(F)** and lateral root number. The STI was calculated by dividing the growth rate measured under salt stress by the growth rate measured under control condition for each accession. **(G)** Na^+/K^+ ratio in root and shoot of different accessions after 10 days on treatment plates. Each dot represents an individual replicate per accession. Lines in (A-C) graphs represent median values. The asterisks above the graphs in (A-C) indicate significant differences between control and salt stress conditions, as determined by the Student 's t-test: *P < 0.05, **P < 0.01, ***P < 0.001, and ****P < 0.0001. Statistical analysis was done by comparison of the means for all pairs using Tukey HSD test for (D-G). Levels not connected by the same letter are significantly different (P < 0.05).

Figure 6. F1 individuals display an increase in main root growth under salt while maintaining lower Na+/K+ ratio in root and shoot. Root system architecture of F1 individuals, their corresponding parents, i.e., cultivated and wild tolerant tomatoes along with wild sensitive tomatoes were investigated with and without 100 mM NaCl. **(A)** Shown are representative images of 9-day-old seedlings that experienced 5 days of salt treatment. Growth rate for **(B)** main root length**, (C)** lateral root length, **(D)** and lateral root number**.** Salt tolerance indexes (STIs) are shown for the **(E)** main root, **(F)** average lateral root length**,** and **(G)** lateral root number. The STI was calculated by dividing the growth rate measured under salt stress by the growth rate measured under control condition for each accession. **(H)** Na^+/K^+ ratio of root and shoot of different accessions after 10 days on treatment plates. Each dot represents individual replicas per accession. Statistical analysis was done by comparison of the means for all pairs using Tukey HSD test in all graphs. Levels not connected by the same letter are significantly different (P < 0.05).

Figure 7. Segregating F2 populations displays four phenotypic bulks for root system architecture. (A) Graph showing root system architecture of 180 F2 individuals alongside their parents under salt stress for lateral root length and lateral root number. The dashed lines used to show the threshold criteria in selecting different bulks, which was 1.8 cm for lateral root length and 10 for the lateral root number. Using these criteria, we identified four phenotypic bulks, as indicated in the figure. **(B)** Representative bulks comparison with most significant changes are shown. Distribution of Δ (SNP index) between the two bulks are shown across the *S. pimpinellifolium* genome. The statistical confidence intervals under the null hypothesis of no QTLs were indicated as green ($p < 0.05$) and blue ($p < 0.01$) lines.

Figure 8. Wild tolerant and cultivated tomatoes show variation in lateral root elongation and emergence under the salt stress. (A) Lateral root length, **(B)** lateral root length growth rate, and **(C)** lateral root number are shown for the two tomato accessions grown in agar plate under 100 mM NaCl. The plates

were imaged using SPIRO setup at a 30-min interval for one week. Individual transparent lines indicate the growth trajectory of individual lateral roots, dashed line indicates the growth average per genotype per condition, whereas the shaded area indicates the standard deviation. The differences between Control and Salt conditions were tested within each genotype using one-way ANOVA, with *, ** and *** representing p-values below 0.05, 0.01 and 0.001, respectively. The growth dynamics of lateral roots were measured over two experimental replicates for 4 biological replicates per genotype per condition.

Figure 9. Differentially expression analyses showing unique and common changes in transcriptome of the two tomato accessions in response to the salt stress. (A) Venn diagrams showing number of differentially expressed genes between the two accessions for all timepoints, and **(B)** across individual time points. **(C)** Intersection of numbers of DEGs under salt treatment relative to control condition across five timepoints. The graphs with orange dots represent DEGs in wild tolerant samples and graphs with blue dots represents cultivated tomato samples. The direction of arrow within each panel represents whether DEGs are significantly up- or down-regulated.

Figure 10. Co-expression network analysis showing distinct patterns among the two accessions across various developmental scales. WGCNA co-expression modules with scaled expression values (y axis) across different time points (x axis) **(A-F).** Black dotted line indicates eigengene expression profile. Gray line indicates expression values of all genes within the module. Most genes in these modules were positively correlated to the eigengene. Genes that are identified through GWAS and BSA (Table 1) and showing significant association with each module were highlighted below their respective modules. See Figure S5 for a detailed analysis of all 14 modules.

Figure 11. Allelic variants analysis revealed the two accessions are almost conserved in their coding sequence but not in the intronic region, as well as 5' and 3' UTRs. (A) Log2 fold changes are shown for the four genes identified by cross-referencing the three experiments, GWAS, BSA, and RNA-Seq, across all developmental time points for the two accessions. Stars indicate statistically significant changes in gene expression, defined as a fold change of ≥ 2 and an adjusted p-value of < 0.05. **(B)** Gene models are illustrated for the four genes, with unique SNP positions depicted as straight lines. The positions of the transcription start site (TSS) and STOP are indicated, with gene locations displayed above. SNPs resulting in missense mutations are depicted along with their corresponding variants in the other accession. See Table S3 for the comprehensive list of variant analyses conducted for the 22 genes identified from GWAS and BSA analyses (Table 1).

Supplemental figures and tables legends

Figure S1. The natural variation in Root System Architecture components in response to salt stress. The 220 genotypes of *S. pimpinellifolium* were germinated on ½ MS agar plates for 4 days and subsequently transferred to media containing 0 or 100 mM NaCl (Control and Salt respectively). The seedlings were imaged every 24 h after transfer for 7 consecutive days. The Root Architecture of seedlings was quantified for the first 4 days after transfer, and inspected for changes throughout time for **(A)** Total Root Size, **(B)** Main Root Length, **(C)** Lateral Root Length, **(D)** Lateral Root Number, **(E)** Center of Gravity (calculated as the position of MR with most Lateral Root Length), and **(F)** ratio of Main Root Length per Total Root Size. The individual lines represent the genotype-specific mean, whereas the dashed lines represent the population average. The *, **, *** and **** represent the significant differences between the treatment at individual time points as tested with two-way ANOVA with p-value < 0.05, 0.01, 0.001 and 0.0001, respectively.

Figure S2. High-confidence loci identified through GWAS. Genome Wide Association Study was performed on 9M SNPs using the standard EMMA-X method. Only SNPs with minor allele frequency > 0.05 were used for plotting the Manhattan plot for associations identified with **(A)** lateral root number at 2 days after transfer to control conditions. The significantly associated loci on chromosome 5, consisting of **(B)** 15 and **(C)** 11 SNPs were inspected in further detail. **(D)** Associations with the number of lateral roots were identified on chromosome 1, and **(E)** the locus consisting of 14 highly associated SNPs has been inspected in more detail. The red line on Manhattan plots indicates the Bonferroni threshold, whereas the blue line indicates genome-wide suggestive threshold. The association graph below each locus represents the association strength with the trait initially associated with that locus.

Figure S3. Wild tomatoes accumulate higher levels of Na+ in the shoot compared to cultivated tomato. (A) Na+ and **(B)** K+ contents of root and shoot of different accessions after 10 days on treatment plates. Each dot represents an individual replicate per accession. Statistical analysis was done by comparison of the means for all pairs using Tukey HSD test. Levels not connected by the same letter are significantly different (P < 0.05).

Figure S4. F1 individuals accumulate less Na+. (A-C) Root system architecture of F1 individuals, their corresponding parents, i.e., cultivated and wild tolerant tomatoes along with wild sensitive tomatoes were investigated with and without 100 mM NaCl. **(D-E)** Na+ and K+ contents of root and shoot of different accessions after 10 days on treatment plates. Each dot represents individual replicas per accession. Statistical analysis was done by comparison of the means for all pairs using Tukey HSD test in all graphs. Levels not connected by the same letter are significantly different (P < 0.05).

Figure S5. Remaining bulk comparisons. Displayed here are the additional BSA results that were not shown in Figure 7.

Figure S6. Intersection of DEGs between WT and CT under Salt and Control conditions. The upset plots highlight the intersection of numbers of DEGs between wild tolerant and cultivated tomato samples

across five timepoints under salt and control conditions, respectively. The panel with dark blue dots represents samples under the control condition, while the panel with brown dots are Salt samples. The direction of arrows within each panel indicates whether the depicted genes are up- or down-regulated.

Figure S7. Co-expression network analysis. The rest of WGCNA co-expression modules are shown here, module 7 to 14.

Figure S8. Gene expression profiles over time for genes identified by overlapping GWAS and BSA analyses in Table 1. Log2 fold changes are shown for the 18 genes identified by cross-referencing the GWAS and BSA, across all developmental time points for the two accessions.

Table S1. Root System Architecture traits for *S. pimpinellifolium* diversity panel. The 89 different phenotypes were recorded for 220 *S. pimpinellifolium* accessions. The traits presented in this table represent the average trait value as calculated based on 4 biological replicates. The trait abbreviations are as follow: aLRL - average Lateral Root Length; aLRLpTRS - ratio of average lateral root length to total root size; CoG - center of gravity calculated as the length of the main root that gives rise to most lateral root biomass; LRL - cumulative lateral root length; LRno - lateral root number, MRL - main root length; MRLpTRS - ratio of main root length to total root size; TRS - total root size. The abbreviations behind the 1st dot indicate either the time and treatment at which individual RSA parameters were recorded (0 - 4 - days post treatment application; C and S for Control and Salt stress respectively), or STI - stress tolerance index - calculated by dividing the trait value recorded under Salt stress conditions by value recorded under Control conditions. GR indicates the growth rate, estimated by fitting a linear curve into change of trait over time.

Table S2. GWAS results. All of the SNPs with -log10(p-value) > 5 ware collated into one table, from two GWAS methods used (ASReml - as used in [30], and EMMA-X). The position of each SNP is indicated in Chr and Pos columns, corresponding to chromosome and position on the chromosome in base pairs as per S.pimpinellifolium genome annotation [36]. The distance between neighboring SNPs is indicated in the "dist" column, and distances below 10,000 bp are highlighted in yellow, while distances below 1,000 bp are highlighted in red. The Pval column indicates the P-value associated with each SNP, and MAF indicates the minor allele frequency of that particular SNP. The trait column indicates the specific trait association used, with aLRL representing average lateral root length, MRL main root length, LRL lateral root length, TRS total root size, perc - a percentage of main root length, CoG - center of gravity calculated for lateral root distribution along the main root length, Apical, Branched and Basal indicating the lengths of individual zones as absolute values or (perc) as percentage of the main root length. The traits recorded under Control conditions are colored in blue, while traits recorded under salt stress are colored with pink. The LOD is calculated as -log10(p-value). The Method represents whether an individual association was observed as significant using ASReml or EMMA-X method.

Table S3. Analysis of allelic variants for the 22 genes that overlap between GWAS and BSA studies.

Table S4. RNA-Seq raw reads and differentially expressed genes (DEGs).

Table S5. Differentially expressed genes (DEGs) for 500 and 4000 minutes.

Table S6. Go enrichment analysis for 500 and 4000 minutes.

References

1. Roșca M, Mihalache G, Stoleru V. Tomato responses to salinity stress: From morphological traits to genetic changes. Front Plant Sci. 2023;14: 1118383. doi:10.3389/fpls.2023.1118383

2. Abrol IP, Yadav JSP, Massoud FI. Salt-affected Soils and Their Management. Food & Agriculture Org.; 1988. Available: https://play.google.com/store/books/details?id=II1HAY-DSGsC

3. Fischer, G., Nachtergaele, O. F, Velthuizen V, T. H, et al. Global Agro-Ecological Zones v4 – Model documentation. Food & Agriculture Org.; 2021. Available: https://play.google.com/store/books/details?id=5X0zEAAAQBAJ

4. Richards LA. Diagnosis and Improvement of Saline and Alkali Soils. United States Department of Agriculture; 1969. Available: https://play.google.com/store/books/details?id=m4BtxgEACAAJ

5. Hassani A, Azapagic A, Shokri N. Global predictions of primary soil salinization under changing climate in the 21st century. Nat Commun. 2021;12: 6663. doi:10.1038/s41467-021-26907-3

6. Cione APP, Schmitt CC, Neumann MG, Gessner F. The Effect of Added Salt on the Aggregation of Clay Particles. J Colloid Interface Sci. 2000;226: 205–209. doi:10.1006/jcis.2000.6812

7. Atkin RK, Barton GE, Robinson DK. Effect of Root-growing Temperature on Growth Substances in Xylem Exudate of Zea mays. J Exp Bot. 1973;24: 475–487. doi:10.1093/jxb/24.2.475

8. Steppuhn H, Raney JP. Emergence, height, and yield of canola and barley grown in saline root zones. Can J Plant Sci. 2005;85: 815–827. doi:10.4141/p04-199

9. Sousa B, Rodrigues F, Soares C, Martins M, Azenha M, Lino-Neto T, et al. Impact of Combined Heat and Salt Stresses on Tomato Plants-Insights into Nutrient Uptake and Redox Homeostasis. Antioxidants (Basel). 2022;11. doi:10.3390/antiox11030478

10. Yang H, Du T, Mao X, Ding R, Shukla MK. A comprehensive method of evaluating the impact of drought and salt stress on tomato growth and fruit quality based on EPIC growth model. Agric Water Manage. 2019;213: 116–127. doi:10.1016/j.agwat.2018.10.010

11. Manaa A, Ben Ahmed H, Valot B, Bouchet J-P, Aschi-Smiti S, Causse M, et al. Salt and genotype impact on plant physiology and root proteome variations in tomato. J Exp Bot. 2011;62: 2797–2813. doi:10.1093/jxb/erq460

12. Morton M, Fiene G, Ahmed HI, Rey E, Abrouk M, Angel Y, et al. Deciphering Salt Stress Responses in Solanum pimpinellifolium through High-Throughput Phenotyping. bioRxiv. 2023. p. 2023.08.15.553433. doi:10.1101/2023.08.15.553433

13. Asins MJ, Bolarín MC, Pérez-Alfocea F, Estañ MT, Martínez-Andújar C, Albacete A, et al. Genetic analysis of physiological components of salt tolerance conferred by Solanum rootstocks. What is the rootstock doing for the scion? Theor Appl Genet. 2010;121: 105–115. doi:10.1007/s00122-010-1294-9

14. Melino V, Tester M. Salt-Tolerant Crops: Time to Deliver. Annu Rev Plant Biol. 2023;74: 671–696. doi:10.1146/annurev-arplant-061422-104322

15. Dempewolf H, Eastwood RJ, Guarino L, Khoury CK, Müller JV, Toll J. Adapting Agriculture to Climate Change: A Global Initiative to Collect, Conserve, and Use Crop Wild Relatives. Agroecology and Sustainable Food Systems. 2014;38: 369–377. doi:10.1080/21683565.2013.870629

16. Ebert AW, Schafleitner R. Utilization of wild relatives in the breeding of tomato and other major vegetables. Crop Wild Relatives and Climate Change. Hoboken, NJ, USA: John Wiley & Sons, Inc; 2015. pp. 141–172. doi:10.1002/9781118854396.ch9

17. Brozynska M, Furtado A, Henry RJ. Genomics of crop wild relatives: expanding the gene pool for crop improvement. Plant Biotechnol J. 2016;14: 1070–1085. doi:10.1111/pbi.12454

18. Li N, He Q, Wang J, Wang B, Zhao J, Huang S, et al. Super-pangenome analyses highlight genomic diversity and structural variation across wild and cultivated tomato species. Nat Genet. 2023;55: 852–860. doi:10.1038/s41588-023-01340-y

19. Pailles Y, Awlia M, Julkowska M, Passone L, Zemmouri K, Negrão S, et al. Diverse Traits Contribute to Salinity Tolerance of Wild Tomato Seedlings from the Galapagos Islands. Plant Physiol. 2020;182: 534–546. doi:10.1104/pp.19.00700

20. Pease JB, Haak DC, Hahn MW, Moyle LC. Phylogenomics Reveals Three Sources of Adaptive Variation during a Rapid Radiation. PLoS Biol. 2016;14: e1002379. doi:10.1371/journal.pbio.1002379

21. Pawełek A, Owusu SA, Cecchetti D, Zielińska A, Wyszkowska J. What evidence exists of crop plants response to exposure to static magnetic and electromagnetic fields? A systematic map protocol. Environ Evid. 2022;11: 1–9. doi:10.1186/s13750-022-00292-w

22. Yassin TE. Inheritance of resistance to leaf curl virus disease in a cross between tomato (Lycopersicon esculentum Mill.) and currant tomato (L. pimpinellifolium (Jusl.) Mill.). J Agric Sci. 1985;105: 659–661. doi:10.1017/S0021859600059566

23. Zhang S, Yu H, Wang K, Zheng Z, Liu L, Xu M, et al. Detection of major loci associated with the variation of 18 important agronomic traits between Solanum pimpinellifolium and cultivated tomatoes. Plant J. 2018;95: 312–323. doi:10.1111/tpj.13952

24. Paran I, van der Knaap E. Genetic and molecular regulation of fruit and plant domestication traits in tomato and pepper. J Exp Bot. 2007;58: 3841–3852. doi:10.1093/jxb/erm257

25. Sarfatti M, Abu-Abied M, Katan J, Zamir D. RFLP mapping of I1, a new locus in tomato conferring resistance against Fusarium oxysporum f. sp. lycopersici race 1. Theor Appl Genet. 1991;82: 22–26. doi:10.1007/BF00231273

26. Celik I, Gurbuz N, Uncu AT, Frary A, Doganlar S. Genome-wide SNP discovery and QTL mapping for fruit quality traits in inbred backcross lines (IBLs) of solanum pimpinellifolium using genotyping by sequencing. BMC Genomics. 2017;18: 1. doi:10.1186/s12864-016-3406-7

27. Ashrafi H, Kinkade M, Foolad MR. A new genetic linkage map of tomato based on a Solanum lycopersicum x S. pimpinellifolium RIL population displaying locations of candidate pathogen response genes. Genome. 2009;52: 935–956. doi:10.1139/g09-065

28. Rao ES, Kadirvel P, Symonds RC, Geethanjali S, Thontadarya RN, Ebert AW. Variations in DREB1A and VP1.1 Genes Show Association with Salt Tolerance Traits in Wild Tomato (Solanum pimpinellifolium). PLoS One. 2015;10: e0132535. doi:10.1371/journal.pone.0132535

29. Wang Z, Hong Y, Zhu G, Li Y, Niu Q, Yao J, et al. Loss of salt tolerance during tomato domestication conferred by variation in a Na+ /K+ transporter. EMBO J. 2020;39: e103256. doi:10.15252/embj.2019103256

30. Awlia M, Alshareef N, Saber N, Korte A, Oakey H, Panzarová K, et al. Genetic mapping of the early responses to salt stress in Arabidopsis thaliana. Plant J. 2021;107: 544–563. doi:10.1111/tpj.15310

31. Kang HM, Sul JH, Service SK, Zaitlen NA, Kong S-Y, Freimer NB, et al. Variance component model to account for sample structure in genome-wide association studies. Nat Genet. 2010;42: 348–354. doi:10.1038/ng.548

32. Ohlsson JA, Leong JX, Elander PH, Dauphinee AN, Ballhaus F, Johansson J, et al. SPIRO – the automated Petri plate imaging platform designed by biologists, for biologists. bioRxiv. 2021. p. 2021.03.15.435343. doi:10.1101/2021.03.15.435343

33. Langfelder P, Horvath S. WGCNA: an R package for weighted correlation network analysis. BMC Bioinformatics. 2008;9: 559. doi:10.1186/1471-2105-9-559

34. Lee MH, Hwang I. Adaptor proteins in protein trafficking between endomembrane compartments in plants. J Plant Biol. 2014;57: 265–273. doi:10.1007/s12374-014-0314-8

35. Abd-Hamid N-A, Ahmad-Fauzi M-I, Zainal Z, Ismail I. Diverse and dynamic roles of F-box proteins in plant biology. Planta. 2020;251: 68. doi:10.1007/s00425-020-03356-8

36. Wang X, Gao L, Jiao C, Stravoravdis S, Hosmani PS, Saha S, et al. Genome of Solanum pimpinellifolium provides insights into structural variants during tomato breeding. Nat Commun. 2020;11: 5817. doi:10.1038/s41467-020-19682-0

37. Kovach MJ, McCouch SR. Leveraging natural diversity: back through the bottleneck. Curr Opin Plant Biol. 2008;11: 193–200. doi:10.1016/j.pbi.2007.12.006

38. Bui HH, Serra V, Pagès L. Root system development and architecture in various genotypes of the Solanaceae family. Botany. 2015;93: 465–474. doi:10.1139/cjb-2015-0008

39. Alaguero-Cordovilla A, Gran-Gómez FJ, Tormos-Moltó S, Pérez-Pérez JM. Morphological Characterization of Root System Architecture in Diverse Tomato Genotypes during Early Growth. Int J Mol Sci. 2018;19. doi:10.3390/ijms19123888

40. Tripodi P, Soler S, Campanelli G, Díez MJ, Esposito S, Sestili S, et al. Genome wide association mapping for agronomic, fruit quality, and root architectural traits in tomato under organic farming conditions. BMC Plant Biol. 2021;21: 481. doi:10.1186/s12870-021-03271-4

41. Ye J, Wang X, Wang W, Yu H, Ai G, Li C, et al. Genome-wide association study reveals the genetic architecture of 27 agronomic traits in tomato. Plant Physiol. 2021;186: 2078–2092. doi:10.1093/plphys/kiab230

42. Hakla HR, Sharma S, Urfan M, Mandlik R, Kumawat S, Rajput P, et al. Genome-Wide Association Study (GWAS) for Identifying SNPs and Genes Related to Phosphate-Induced Phenotypic Traits in Tomato (Solanum lycopersicum L.). Plants. 2024;13. doi:10.3390/plants13030457

43. Rodriguez M, Scintu A, Posadinu CM, Xu Y, Nguyen CV, Sun H, et al. GWAS Based on RNA-Seq SNPs and High-Throughput Phenotyping Combined with Climatic Data Highlights the Reservoir of Valuable Genetic Diversity in Regional Tomato Landraces. Genes . 2020;11. doi:10.3390/genes11111387

44. Julkowska MM, Koevoets IT, Mol S, Hoefsloot H, Feron R, Tester MA, et al. Genetic Components of Root Architecture Remodeling in Response to Salt Stress. Plant Cell. 2017;29: 3198–3213. doi:10.1105/tpc.16.00680

45. Munns R, Tester M. Mechanisms of salinity tolerance. Annu Rev Plant Biol. 2008;59: 651–681. doi:10.1146/annurev.arplant.59.032607.092911

46. Neuteboom LW, Veth-Tello LM, Clijdesdale OR, Hooykaas PJ, van der Zaal BJ. A novel subtilisin-like protease gene from Arabidopsis thaliana is expressed at sites of lateral root emergence. DNA Res. 1999;6: 13–19. doi:10.1093/dnares/6.1.13

47. Ahanger MA, Tomar NS, Tittal M, Argal S, Agarwal RM. Plant growth under water/salt stress: ROS production; antioxidants and significance of added potassium under such conditions. Physiol Mol Biol Plants. 2017;23: 731–744. doi:10.1007/s12298-017-0462-7

48. Wang J, Yu Y, Zhang Z, Quan R, Zhang H, Ma L, et al. Arabidopsis CSN5B interacts with VTC1 and modulates ascorbic acid synthesis. Plant Cell. 2013;25: 625–636. doi:10.1105/tpc.112.106880

49. Dinneny JR. Developmental Responses to Water and Salinity in Root Systems. Annu Rev Cell Dev Biol. 2019;35: 239–257. doi:10.1146/annurev-cellbio-100617-062949

50. Thabet SG, Moursi YS, Sallam A, Karam MA, Alqudah AM. Genetic associations uncover candidate SNP markers and genes associated with salt tolerance during seedling developmental phase in barley. Environ Exp Bot. 2021;188: 104499. doi:10.1016/j.envexpbot.2021.104499

51. Hasanuzzaman M, Bhuyan MHMB, Anee TI, Parvin K, Nahar K, Mahmud JA, et al. Regulation of Ascorbate-Glutathione Pathway in Mitigating Oxidative Damage in Plants under Abiotic Stress. Antioxidants (Basel). 2019;8. doi:10.3390/antiox8090384

52. Shalata A, Neumann PM. Exogenous ascorbic acid (vitamin C) increases resistance to salt stress and reduces lipid peroxidation. J Exp Bot. 2001;52: 2207–2211. doi:10.1093/jexbot/52.364.2207

53. Zhang Z, Wang J, Zhang R, Huang R. The ethylene response factor AtERF98 enhances tolerance to salt through the transcriptional activation of ascorbic acid synthesis in Arabidopsis. Plant J. 2012;71: 273–287. doi:10.1111/j.1365-313X.2012.04996.x

54. [No title]. [cited 23 May 2024]. Available: https://academic.oup.com/plphys/article/143/2/707/6106670

55. Achard P, Cheng H, De Grauwe L, Decat J, Schoutteten H, Moritz T, et al. Integration of plant responses to environmentally activated phytohormonal signals. Science. 2006;311: 91–94.

doi:10.1126/science.1118642

56. Peng J, Li Z, Wen X, Li W, Shi H, Yang L, et al. Salt-induced stabilization of EIN3/EIL1 confers salinity tolerance by deterring ROS accumulation in Arabidopsis. PLoS Genet. 2014;10: e1004664. doi:10.1371/journal.pgen.1004664

57. Jiang C, Belfield EJ, Cao Y, Smith JAC, Harberd NP. An Arabidopsis soil-salinity-tolerance mutation confers ethylene-mediated enhancement of sodium/potassium homeostasis. Plant Cell. 2013;25: 3535–3552. doi:10.1105/tpc.113.115659

58. Lobet G, Pagès L, Draye X. A novel image-analysis toolbox enabling quantitative analysis of root system architecture. Plant Physiol. 2011;157: 29–39. doi:10.1104/pp.111.179895

59. Wickham H. ggplot2: Elegant Graphics for Data Analysis. Springer; 2016. Available: https://play.google.com/store/books/details?id=XgFkDAAAQBAJ

60. Wickham H, Averick M, Bryan J, Chang W, McGowan L, François R, et al. Welcome to the tidyverse. J Open Source Softw. 2019;4: 1686. doi:10.21105/joss.01686

61. Wilke CO. cowplot: streamlined plot theme and plot annotations for “ggplot2.” CRAN Repos. 2016.

62. Wickham H. reshape2: flexibly reshape data: a reboot of the reshape package. R package version. 2020.

63. Keitt T. Builds Color Tables [R package colorRamps version 2.3.4]. [cited 5 Jun 2024]. Available: https://cran.r-project.org/web/packages/colorRamps/index.html

64. doBy: Groupwise Statistics, LSmeans, Linear Estimates, Utilities. In: Comprehensive R Archive Network (CRAN) [Internet]. [cited 5 Jun 2024]. Available: https://cran.r-project.org/web/packages/doBy/index.html

65. Sievert C. Interactive Web-Based Data Visualization with R, plotly, and shiny. CRC Press; 2020. Available: https://play.google.com/store/books/details?id=7zPNDwAAQBAJ

66. Kassambara A. ggpubr:’ggplot2'Based Publication Ready Plots. R package version 0.4. 0.] https://cran-r-project org/web/packages/ggpubr/indes ….

67. Wei T, Simko V. R package“ corrplot”: Visualization of a Correlation Matrix (Version 0.84). Retrived from, https://github com/taiyun/corrplot. 2017.

68. Categorical Scatter (Violin Point) Plots [R package ggbeeswarm version 0.7.2]. 2023 [cited 5 Jun 2024]. Available: https://cran.r-project.org/web/packages/ggbeeswarm/index.html

69. Chen B. Access Data from the USDA ARMS Data API [R package rarms version 1.0.0]. 2020. Available: https://cran.r-project.org/web/packages/gapminder/index.html

70. Wang J, Zhang Z. GAPIT Version 3: Boosting Power and Accuracy for Genomic Association and Prediction. Genomics Proteomics Bioinformatics. 2021;19: 629–640. doi:10.1016/j.gpb.2021.08.005

71. Bolger AM, Lohse M, Usadel B. Trimmomatic: a flexible trimmer for Illumina sequence data. Bioinformatics. 2014;30: 2114–2120. doi:10.1093/bioinformatics/btu170

72. Li H. Aligning sequence reads, clone sequences and assembly contigs with BWA-MEM. arXiv [q-bio.GN]. 2013. Available: http://arxiv.org/abs/1303.3997

73. McKenna A, Hanna M, Banks E, Sivachenko A, Cibulskis K, Kernytsky A, et al. The Genome Analysis Toolkit: a MapReduce framework for analyzing next-generation DNA sequencing data. Genome Res. 2010;20: 1297–1303. doi:10.1101/gr.107524.110

74. Takagi H, Abe A, Yoshida K, Kosugi S, Natsume S, Mitsuoka C, et al. QTL-seq: rapid mapping of quantitative trait loci in rice by whole genome resequencing of DNA from two bulked populations. Plant J. 2013;74: 174–183. doi:10.1111/tpj.12105

75. Kim D, Paggi JM, Park C, Bennett C, Salzberg SL. Graph-based genome alignment and genotyping with HISAT2 and HISAT-genotype. Nat Biotechnol. 2019;37: 907–915. doi:10.1038/s41587-019-0201-4

76. Liao Y, Smyth GK, Shi W. featureCounts: an efficient general purpose program for assigning sequence reads to genomic features. Bioinformatics. 2014;30: 923–930. doi:10.1093/bioinformatics/btt656

77. Love M, Anders S, Huber W. Differential analysis of count data – the DESeq2 package. 2013. Available: https://cdimage.debian.org/mirror/bioconductor.org/packages/3.3/bioc/vignettes/DESeq2/inst/doc/DESeq2.pdf

78. Conway JR, Lex A, Gehlenborg N. UpSetR: an R package for the visualization of intersecting sets and their properties. Bioinformatics. 2017;33: 2938–2940. doi:10.1093/bioinformatics/btx364

79. Conesa A, Götz S. Blast2GO: A comprehensive suite for functional analysis in plant genomics. Int J Plant Genomics. 2008;2008: 619832. doi:10.1155/2008/619832